Modulation of Wind-Work by Oceanic Current Interaction with the Atmosphere

Lionel Renault, M. Jeroen Molemaker, James C. Mcwilliams, Alexander Shchepetkin, Florian Lemarié, Dudley Chelton, Serena Illig, Alex Hall

▶ **To cite this version:**

Lionel Renault, M. Jeroen Molemaker, James C. Mcwilliams, Alexander Shchepetkin, Florian Lemarié, et al.. Modulation of Wind-Work by Oceanic Current Interaction with the Atmosphere. Journal of Physical Oceanography, 2016, 46 (6), pp.1685-1704. 10.1175/JPO-D-15-0232.1 . hal-01295496

HAL Id: hal-01295496
https://inria.hal.science/hal-01295496

Submitted on 31 Mar 2016

HAL is a multi-disciplinary open access archive for the deposit and dissemination of scientific research documents, whether they are published or not. The documents may come from teaching and research institutions in France or abroad, or from public or private research centers.

L'archive ouverte pluridisciplinaire **HAL**, est destinée au dépôt et à la diffusion de documents scientifiques de niveau recherche, publiés ou non, émanant des établissements d'enseignement et de recherche français ou étrangers, des laboratoires publics ou privés.

Modulation of Wind-Work by Oceanic Current Interaction with the Atmosphere

Lionel Renault[(1)]*, Jeroen Molemaker[(1)], James C. McWilliams[(1)], Alexander F. Shchepetkin[(1)], Florian Lemarié[(2)], Dudley Chelton[(3)], Serena Illig[(4)], Alex Hall[(1)]

(1) Department of Atmospheric and Oceanic Sciences, University of California, Los Angeles, California, USA

(2) INRIA, Univ. Grenoble-Alpes, CNRS, LJK, F-38000 Grenoble, France

(3) College of Earth, Ocean, and Atmospheric Sciences, Oregon State University, Oregon, USA

(4) Laboratoire d'Étude en Géophysique et Océanographie Spatiale, IRD, Toulouse, France

Corresponding author address: Lionel Renault, Department of Atmospheric and Oceanic Sciences, University of California, Los Angeles, 405 Hilgard Ave., Los Angeles, CA 90095-1565.

E-mail: lrenault@atmos.ucla.edu

ABSTRACT

In this study, uncoupled and coupled ocean-atmosphere simulations are carried out over the California Upwelling System to assess the dynamic ocean-atmosphere interactions, *viz.,*the ocean surface current feedback to the atmosphere. We show the current feedback, by modulating the energy transfer from the atmosphere to the ocean, controls the oceanic Eddy Kinetic Energy (EKE), and for the first time, we demonstrate the current feedback has an opposite effect on the surface stress and on the wind itself. The current feedback acts as an oceanic eddy killer, reducing by half the Surface EKE, and by 27% the depth-integrated EKE. On one hand, it reduces the coastal generation of eddies by weakening the nearshore supply of positive wind work. On the other hand, offshore, it removes energy from the geostrophic current into the atmosphere, damping eddies. A negative feedback on the surface stress explains the coastal reduction of energy transfer from the atmosphere to the ocean and an offshore return of energy from the ocean to the atmosphere, partially re-energizing the atmosphere. This, in turn, partly re-energizes the ocean by increasing the coastal transfer of energy from the atmosphere and by inducing an opposite wind curl, decreasing the offshore return of energy to the atmosphere. Eddy statistics confirm the current feedback damps the eddies and reduces their lifetime, improving the realism of the simulation. Finally, we propose an additional energy element in the Lorenz diagram of energy conversion, *viz.,*the current-induced transfer of energy from the ocean to the atmosphere at the eddy scale.

1. Introduction

Eastern Boundary Upwelling Systems (EBUS), such as the California Current System (CCS), belong to the most productive coastal environments (*e.g.,* Carr and Kearns 2003), supporting some of the world's major fisheries (*e.g.,* FAO 2009). The CCS upwelling and productivity present a seasonal variability with a favorable season during spring and summer (Marchesiello et al. 2003, Renault et al. 2015b), where high biological productivity is largely determined by wind-driven upwelling. As for the other EBUS (*e.g.,* Benguela, Canary and Humboldt), equatorward winds drive coastal upwelling, Ekman pumping, alongshore currents and then productivity. Additionally, coastal currents and significant oceanic mesoscale variability contribute to cross-shore exchange of heat, salt, and biogeochemical tracers between the open and coastal oceans (Marchesiello et al. 2003, Capet et al. 2008b, Gruber et al. 2011, Chaigneau et al. 2011).

Eddies generated by dynamical instabilities of the currents (Marchesiello et al. 2003) lead to lateral heat transport, so that effects of coastal upwelling on Sea Surface Temperature (SST) can be felt hundreds of km away (Capet et al. 2008b). In the open ocean, and in particular in low-nutrient environments, mesoscale processes increase the net upward flux of limiting nutrients and enhance biological production (Martin and Richards 2001; McGillicuddy et al. 2007). For the EBUS, as shown by *e.g.,* Carr and Kearns (2003), the Net Primary Production (NPP) is primarily controlled by the magnitude of the upwelling favorable winds through the upwelling strength. However, Lathuilière et al. (2010), Gruber et al. (2011), and Renault et al. (2015a) also show that eddies can be a limiting factor, which progressively prevent high levels of NPP as the number of eddies increase by subducting the

nutrient below the euphotic layer ("eddy quenching"). Renault et al. (2015a) show that the coastal wind shape, by modulating the baroclinic instabilities, modulates the Eddy Kinetic Energy (EKE) and therefore the eddy quenching. The eddy contribution to oceanic fluxes is substantial (Colas et al. 2013), and a realistic wind forcing is crucial to simulate the mesoscale activity realistically (Renault et al. 2015a).

In the EBUS, various processes can modulate the spatial pattern of the wind, *e.g.,* sharp changes of surface drag and atmospheric boundary layer at the land-sea interface (Edwards et al. 2001, Capet et al. 2004, Renault et al. 2015b), coastal orography (Edwards et al. 2001, Perlin et al. 2011, Renault et al. 2015b), and SST-wind coupling (Chelton et al. 2007, Jin et al. 2009). Renault et al. 2015b and Renault et al. 2015a show that the coastal wind shape in the CCS is mainly controlled by the orography. These coastal circulation processes are essential for understanding the upwelling systems (Marchesiello et al. 2003, Capet et al. 2004, Renault et al. 2012). The ocean feedback to the atmosphere has been recently studied, mainly focusing on the thermal feedback (*e.g.,* Chelton et al. 2004, Chelton et al. 2007, Spall 2007, Perlin et al. 2007, 2011,Minobe et al. 2008, Jin et al. 2009, Park et al. 2006, Cornillon and Park 2001). SST gradients induce gradients in lower-atmospheric stratification; hence, gradients in vertical momentum flux in the atmospheric boundary layer and gradients in the surface wind and stress are induced beneath an otherwise more uniform mid-tropospheric wind. Chelton et al. (2004) and Chelton et al. (2007), using satellite observations, show approximately linear relationships between the surface stress curl and divergence and the crosswind and downwind components of the local SST gradient. Recent studies also highlight how a mesoscale SST front may have an impact up to the troposphere (Minobe et al. 2008). The effect of oceanic currents is another aspect of interaction between atmosphere and ocean;

however, its effects are not yet well known. Some work shows that the current effect on the surface stress can lead to a reduction of the EKE of the ocean via a "mechanical damping" (Duhaut and Straub 2006; Dewar and Flierl 1987; Dawe and Thompson 2006; Hughes and Wilson 2008; Eden and Dietze 2009) and hence a reduction of the wind work. However, in those studies the atmospheric response to the current feedback is neglected. Recently, Seo et al. (2015), using coupled model, confirms the current feedback induces a reduction of the wind work, that in turn, damps the EKE. To our knowledge, the effects of surface currents on the surface wind speed has not been yet studied. Eden and Dietze (2009) can be associated with an observational analysis that shows that the current-induced surface stress curl change induces Ekman pumping velocities that are of the opposite sign to the surface vorticity of the eddy, inducing its attenuation (Gaube et al. 2015).

In oceanic numerical modeling, the surface stress is usually estimated as a function of the wind speed, ignoring the fact that the current also has a drag force on the atmosphere. Scott and Xu (2009) shows such a simplification can lead to an overestimation of the total energy input to the ocean by wind work and suggests the current should be included when estimating the surface stress. In this paper, using a set of coupled and partially coupled simulations, the focus is on this surface current feedback to the atmosphere. The objectives are to assess how the current feedback modifies the wind work and to address how it alters both the atmospheric and oceanic EKE. This raises the question of how best to force an oceanic model. Oceanic simulations forced by a prescribed wind stress inherently cannot represent the current feedback on the stress. Furthermore, although uncoupled oceanic simulations forced by an atmospheric wind product can estimate the surface stress using the air-sea velocity difference, they cannot represent the influence of surface currents on the

surface wind speed, to our knowledge, this point has not previously been documented

The paper is organized as follows: Section 2 describes the model configuration and methodology. In Sec. 3, the effect of the current feedback on the surface stress and EKE is assessed. Section 4 addresses the corresponding wind adjustment. In Sec. 5 an eddy attenuation time scale and Ekman pumping are estimated, and a mechanistic view of the current feedback effect is presented. In Sec. 6 an eddy statistical view allows a direct validation of our results by comparison to observations. The results are discussed in Sec. 7, which is followed by the conclusions.

2. Model Configuration and Methodology

a. The Regional Oceanic Modeling System (ROMS)

The oceanic simulations were performed with the Regional Oceanic Modeling System (ROMS) (Shchepetkin and McWilliams 2005) in its AGRIF (Adapted Grid Refinement in Fortran) version) (Debreu et al. 2012). ROMS is a free-surface, terrain-following coordinate model with split-explicit time stepping and Boussinesq and hydrostatic approximations. ROMS is implemented in a configuration with two offline nested grids. The coarser grid extends from 170°W to 104°W and from 18°N to 62.3°N along the U.S. West Coast and is 322 x 450 points with a resolution of 12 km. Its purpose is to force the second domain. The second domain grid extends from 144.7°W to 112.5°W and from 22.7°N to 51.1°N (Fig. 1). The model grid is 437 x 662 points with a resolution of 4 km. The boundary condition algorithm consists of a modified Flather-type scheme for the barotropic mode (Mason et al.

2010) and Orlanski-type scheme for the baroclinic mode (including T and S; Marchesiello et al. 2001).

Bathymetry for all domains is constructed from the Shuttle Radar Topography Mission (SRTM30 plus) dataset (available online at http://topex.ucsd.edu/WWW˙html/srtm30˙plus.html) based on the 1-min Sandwell and Smith (1997) global dataset and higher-resolution data where available. A Gaussian smoothing kernel with a width of 4 times the topographic grid spacing is used to avoid aliasing whenever the topographic data are available at higher resolution than the computational grid and to ensure the smoothness of the topography at the grid scale. The slope parameter ($r = \Delta h/2\overline{h}$) is a ratio of the maximum difference between adjacent grid cell depths and the mean depth at that point, used to assess the potential impact of errors induced by terrain-following (s-coordinate) horizontal layers. In regions with steep terrain combined with shallow depths, a relatively small rmax is necessary to prevent pressure gradient errors which result in artificial currents developing from a state of rest with no forcing (Beckmann and Haidvogel 1993) Here, local smoothing is applied where the steepness of the topography exceeds a factor $rmax = 0.2$.

Lateral oceanic forcing for the largest domain as well as surface forcing for all simulations are interannual. Temperature, salinity, surface elevation, and horizontal velocity initial and boundary information for the largest domain covering the whole North America West Coast are taken from the monthly averaged Simple Ocean Data Assimilation (SODA) ocean interannual outputs (Carton and Giese 2008). A bulk formulae (Large 2006) is used to estimate the freshwater, turbulent, and momentum fluxes using the atmospheric fields derived from the uncoupled WRF simulation. In the coupled simulations, the fluxes are computed by WRF and then given to ROMS using the same bulk formulae.

The 12 km domain is first spun up from the SODA initial state the 1st January 1994 for a few months, then run for an additional period until end of 1999. Kinetic energy in the domain is statistically equilibrated within the first few months of simulation. The second grid (4 km resolution) is then nested in the parent grid from 1st June 1994. Results obtained after a 6-month spin-up are then used in our analysis. All domains have 42 levels in the vertical with the same vertical grid system concentrating vertical levels near the surface (Shchepetkin and McWilliams 2009), with stretching surface and bottoms parameters $hcline = 250\ m$, $\theta b = 1.5$, and $thetas = 6.5$. Finally, vertical mixing of tracers and momentum is done with a K-profile parameterization (KPP; Large et al. 1994). In this study, only the period 1995-1999 is analyzed.

b. The Weather Research and Forecast (WRF) Model

WRF (version 3.6, Skamarock et al. 2008) is implemented in a configuration with two nested grids. The largest domain covers the North American West Coast with a horizontal resolution of 18 km (not shown); the inner domain covers the U.S. West Coast, with a horizontal resolution of 6 km (see Renault et al. 2015b), that is slightly larger than the ROMS 4 km grid. The coarser grid (WRF18) reproduces the large-scale synoptic features that force the local dynamics in the second grid, each using a one-way offline nesting with three-hourly updates of the boundary conditions. The coarser grid simulation (WRF18) was first run independently. It is initialized with the Climate Forecast System Reanalysis (CFSR) ($\approx 40\,km$ spatial resolution; Saha et al. 2010) from 1rd January 1994 and integrated for 6 years with time-dependent boundary conditions interpolated from the same three-hourly

reanalysis. Forty vertical levels are used, with half of them in the lowest 1.5 km. The nested domain (WRF6) was initialized from the coarse solution WRF18 on 1rd June 1994 and integrated 5.5 years.

A full set of parameterization schemes is included in WRF. The model configuration was setup with the following parameterizations: the WRF Single-Moment 6-class microphysics scheme (Hong and Lim 2006) modified to take into account the droplet concentration (Jousse et al. 2015); the Tiedtke cumulus parameterization (Zhang et al. 2011); the new Goddard scheme for shortwave and longwave radiation (Chou and Suarez 1999) the Noah land surface model (Skamarock et al. 2008); and the MYNN2.5 planetary boundary layer (PBL) scheme (Nakanishi and Niino 2006).[1]

c. OASIS/MCT Coupling Procedure

The OASIS coupler (`https://verc.enes.org/oasis/metrics/oasis4-dissemination`), which is based on MCT (Model Coupling Toolkit; developed at Argonne National Lab) and supports exchanges of general two-dimensional fields between numerical codes representing different components of the climate system. All transformations, including regridding, are executed in parallel on the set of source or target component processes, and all coupling exchanges are executed in parallel directly between the components. In our configuration, every hour, WRF gives to ROMS the hourly averages of freshwater, heat, and momentum fluxes, whereas ROMS sends to WRF the hourly SST

[1]Other WRF PBL schemes were tried (*e.g.,* Yonsei University YSU, (Hong et al. 2006), University of Washington, Park and Bretherton (2009)). The MYNN2.5 gave in general more realistic features, especially in terms of cloud cover.

and eventually, the surface currents.

d. Experiments

Table 1 summarizes the three experiments carried out to assess the impact of the oceanic currents on the surface stress, the wind, and the oceanic EKE. EXP1 is a SST coupled ROMS-WRF simulation. EXP2 is an uncoupled simulation that uses the atmosphere from EXP1 and that takes into account the oceanic surface current when estimating the surface stress. It allows us to assess the oceanic response to the current feedback. Finally, EXP3 is a fully coupled simulation in the sense that it has both thermal and current feedbacks to the atmosphere. The surface stress is estimated using a bulk formula with a velocity that is the wind relative to the current:

$$\boldsymbol{U} = \boldsymbol{U_a} - \boldsymbol{U_o}, , \tag{1}$$

where $\boldsymbol{U_a}$ and $\boldsymbol{U_o}$ are the surface wind (at the first vertical level in WRF) and the surface current, respectively. As described by Lemarié (2015), because of the implicit treatment of the bottom boundary condition in most atmospheric models, the use of relative winds involves a modification of both the surface-layer vertical mixing parameterization (MYNN2.5 in our case) and the tridiagonal matrix for vertical turbulent diffusion.

e. EKE Budget

All quantities are decomposed into a 1995-1999 time mean (overbar,"") and deviations (primes, "′"). In our analysis the seasonal variability is not removed.

The total wind work is defined as

$$FK = \frac{1}{\rho_0} \left(\overline{\tau_x \, u_o} + \overline{\tau_y \, v_o} \right), \tag{2}$$

where u_o and v_o are the zonal and meridional surface currents, τ_x and τ_y are the zonal and meridional surface stresses, and ρ_0 is mean seawater density.

The geostrophic wind work is defined as

$$FK_g = \frac{1}{\rho_0} \left(\overline{\tau_x \, u_{og}} + \overline{\tau_y \, v_{og}} \right), \tag{3}$$

where u_{og} and v_{og} are the zonal and meridional surface geostrophic currents.

As in Marchesiello et al. (2003), we focus on the following relevant energy source and eddy-mean conversion terms:

- The mean wind work:

$$F_m K_m = \frac{1}{\rho_0} \left(\overline{\tau_x} \, \overline{u_o} + \overline{\tau_y} \, \overline{v_o} \right). \tag{4}$$

- The eddy wind work:

$$F_e K_e = \frac{1}{\rho_0} \left(\overline{\tau'_x \, u'_o} + \overline{\tau'_y \, v'_o} \right). \tag{5}$$

- Barotropic (Reynolds stress) conversion $K_m K_e$:

$$K_m K_e = \int_z -(\overline{u'_o \, u'_o} \frac{\partial \overline{u_o}}{\partial x} + \overline{u'_o \, v'_o} \frac{\partial \overline{u_o}}{\partial y} + \overline{u'_o \, w'} \frac{\partial \overline{u_o}}{\partial z} + \overline{v'_o \, u'_o} \frac{\partial \overline{v_o}}{\partial x} + \overline{v'_o \, v'_o} \frac{\partial \overline{v_o}}{\partial y} + \overline{v'_o \, w'} \frac{\partial \overline{v_o}}{\partial z}), \tag{6}$$

  where w is the vertical velocity and x, y, and z are the zonal, meridional, and vertical coordinates, respectively.

- Baroclinic conversion $P_e K_e$:

$$P_e K_e = \int_z -\frac{g}{\rho_0} \overline{\rho' \, w'}, \tag{7}$$

  where g is the gravitational acceleration.

F_mK_m represents the transfer of energy from mean surface wind-forcing to mean Kinetic Energy, F_eK_e represents the transfer of energy from surface wind-forcing anomalies to EKE, K_mK_e represents the barotropic conversion from mean kinetic energy to EKE, and $PeKe$ represents the baroclinic conversion from eddy available potential energy to EKE. We computed those conversion terms at each model grid point. The anomalies are estimated with respect to the long-term means. The wind work is estimated at the free surface, whereas the barotropic and baroclinic conversion terms are integrated over the whole water column. In the following, cross-shore sections are evaluated using d as the cross-shore distance.

f. Eddy Tracking

The eddy tracking detection method developed by Chelton et al. (2011) is used to detect and track eddies in the simulations and in the AVISO dataset (Ducet et al. 2000). This approach consists of detecting closed contours of Sea Level Anomalies (SLA) that include a local extremum and several other criteria to identify and track mesoscale eddies. An eddy is viewed as a coherent isolated vortex and therefore the corresponding SLA has the form of a bump or a depression. Before applying the eddy tracking procedure, the model outputs were first filtered by removing the seasonal cycle (annual plus semiannual components) at each grid point. In this study, we define the long-lived eddies as tracked eddies that have a continuous lifetime greater than 16 weeks. The AVISO data are only able to resolve eddies with radii longer than about 40 km (Chelton et al. 2011). However, although the eddy lifetime dependence on eddy scale in the real ocean is not yet known, by focusing on eddies with long lifetimes, the resolution capability of the AVISO dataset should not be a major

limitation.

3. Eddy Kinetic Energy and Energy Conversion

a. Eddy Kinetic Energy

The surface EKE from the different experiments is estimated using the daily surface current perturbations. The mean surface EKE and the temporal evolution of its domain-average are in Fig. 1. In good agreement with the literature (Marchesiello et al. 2003; Renault et al. 2015a), in all the experiments the EKE has larger values not too far offshore and exhibits a broad decay further offshore. EXP1 shows a relatively weak decay with high values of EKE offshore. From EXP1 to EXP2, the current feedback to the surface stress reduces the EKE by 55%, and in particular, it strongly decreases the offshore EKE, improving the realism of the simulation (*e.g.,* see Fig. 2 from Capet et al. 2008a). EXP3 also reduces the surface EKE relative to EXP1, but only by 40%, which is in good agreement with Seo et al. 2015. The atmospheric response to the reduced wind work with current feedback leads to an increase in surface wind strength (see Section 4b), hence the EKE reduction observed in EXP2 is diminished. To our knowledge, this is the first time this phenomenon has been documented. Similar conclusions can be drawn using the depth-integrated EKE: from EXP1 to EXP2, it is reduced by 35%, whereas, from EXP1 to EXP3, it is reduced by only 27 %. The exclusion of an atmospheric response in EXP2 leads to an overestimation of the oceanic EKE reduction, both nearshore and offshore. The EKE reduction can be split into two processes. On one hand, there is a surface stress adjustment that tends to reduce

the EKE (EXP2). On the other hand, there is a wind adjustment that partly counteracts the surface stress reduction, thus attenuating the EKE reduction (EXP3).

b. Energy Conversion

A simplified EKE budget (Sec. 2e) is computed to diagnose which processes lead to the EKE reduction by the current feedback. Since the time-mean quantities and then $F_m K_m$ are barely affected by the current feedback (about 1% change, not shown), Fig. 2 shows the spatial distribution of only $F_e K_e$, $P_e K_e$, and $K_m K_e$ from EXP1 (top panel) and EXP3 (bottom panel), and Fig. 3 is the cross-shore profile for each term averaged between 30°N and 45°N from EXP1, EXP2, and EXP3. As in Marchesiello et al. (2003), the baroclinic instability and the eddy wind work are the main sources of EKE, and they have higher values in the nearshore region. Note, here, that $K_m K_e$ is a secondary term. The wind work is also stronger in those simulations than in Marchesiello et al. (2003), which can be attributed to the poor quality of the wind used in Marchesiello et al. (2003) (*i.e.,* COADS): it is monthly, and in particular it does not resolve the high frequency wind forcing (hourly here, which excites inertial currents) nor the slackening of the winds near the coast (drop-off, *e.g.,* Renault et al. 2015a). The COADS wind stress forcing induces too low levels of EKE. As in Marchesiello et al. (2003), in the nearshore region, a coastal band of about $80\,km$ width is marked by a large values of $F_e K_e$. In all the experiments, the wind perturbations induce an offshore Ekman surface current and an oceanic coastal jet (*e.g.,* Renault et al. 2009) that flows partly in the same direction as the wind, inducing a positive $F_e K_e$. Also offshore, the Ekman surface current is partly in the direction of the wind with a generally

positive F_eK_e.

The main effect of the current feedback is a reduction of F_eK_e in both the nearshore and offshore regions (Figs. 2 and 3). The oceanic surface current can be split into their geostrophic and ageostrophic parts:

$$u_o = u_{og} + u_{oa} \tag{8}$$

and

$$v_o = v_{og} + v_{oa}\,, \tag{9}$$

with u_{og}, v_{og}, u_{oa}, and v_{oa} the zonal and meridional geostrophic and ageostrophic currents, respectively. Using (8) and (9), F_eK_e can in turn be split into its geostrophic (F_eK_{eg}) and ageostrophic (F_eK_{ea}) parts:

$$F_eK_{eg} = \frac{1}{\rho_0}\left(\overline{\tau'_x\,u'_{og}} + \overline{\tau'_y\,v'_{og}}\right) \tag{10}$$

and

$$F_eK_{ea} = \frac{1}{\rho_0}\left(\overline{\tau'_x\,u'_{oa}} + \overline{\tau'_y\,v'_{oa}}\right). \tag{11}$$

Figure 4 shows F_eK_{eg} from EXP1 and EXP3, and Fig. 3c shows the cross-shore profile of F_eK_{eg} from EXP1, EXP2, and EXP3. In all the experiments, the offshore positive F_eK_e is essentially due to F_eK_{ea} (more than 95%), whereas, nearshore, F_eK_{ea} accounts for only 37% of F_eK_e.

The induced current feedback reduction of F_eK_e mainly acts through the geostrophic currents. Offshore, the current-induced reduction of F_eK_e is due to two different mechanisms: 1) a slight reduction of its ageostrophic part F_eK_{ea} (3%; Fig. 3), that is explained by changes in Ekman induced surface current. 2) a sink of energy through its geostrophic part F_eK_{eg}

285 (actual negative values of F_eK_{eg}). In that sense the current feedback acts as an "eddy
286 killer". Figure 5 illustrates the geostrophic sink through F_eK_{eg} for an anticyclonic eddy
287 with a southward uniform wind blowing up over such an eddy. In EXP1, over such an eddy,
288 F_eK_{eg} is equal to zero. There is a positive F_eK_{eg} on the eastern branch and a negative
289 F_eK_{eg} on the western branch, with a uniform wind, the net F_eK_{eg} is zero. In EXP2, the
290 wind is still uniform since it does not react to the current feedback. However, the eastern
291 branch has the currents acting in the same direction as the wind, and hence has a reduced
292 surface stress, $\tau = C_d\,\rho_a\,(U_a - U_o)^2 < C_d\,\rho_a\,(U_a)^2$ (C_d is the drag coefficient), whereas the
293 western branch has the currents acting against the wind, and hence an increased surface
294 stress, $\tau = C_d\,\rho_a\,(U_a - U_o)^2 > C_d\,\rho_a\,U_a^2$. As a result, the positive (negative) part of F_eK_{eg} is
295 reduced (increased), and the net F_eK_{eg} becomes negative, deflecting energy from the ocean
296 to the atmosphere. In EXP3, the current feedback not only acts on the surface stress but also
297 on the atmosphere and, in particular on the wind. The wind response damps the efficiency of
298 the F_eK_{eg} sink, explaining the damping of the offshore EKE reduction from EXP2 to EXP3
299 shown in Fig. 1. On the eastern branch of the eddy, there is less friction and more energy
300 in the atmosphere, so that the wind can accelerate, increasing the relative wind and hence
301 increasing back F_eK_{eg}. On the western branch, there is more friction, that leads to a decrease
302 of the wind, but also more energy, that should lead to an increase of the wind. On average,
303 as shown in Sec. 4, it leads to a decrease of the wind and hence to a less negative F_eK_{eg}.
304 The net F_eK_{eg} in EXP3 is still negative but less than EXP2, the atmospheric response tends
305 to re-energize the ocean.

306 In the coastal band of $80\,km$ width, there is a reduction of energy input through F_eK_{eg}.
307 As for the offshore region, the presence of eddies weakens the wind work. However, the wind

perturbations also induce an oceanic geostrophic coastal jet that blows partially toward the same direction as the wind. Hence, the relative wind $U = U_a - U_o$ taken into account to estimate the surface stress in EXP2 and EXP3 is weaker than the absolute wind U_a used in EXP1 to estimate the stress. As a result the stress perturbations are reduced in EXP2 and EXP3 with respect to EXP1, reducing F_eK_{eg} (Fig. 6). In EXP3, as for the offshore region, the atmospheric response damps the current-induced surface stress reduction by changing the wind (Fig. 5 and . 6).

To sum up, although the atmospheric response tends to re-energize the ocean, the current feedback to the atmosphere acts as an eddy killer and induces an energy sink from the ocean to the atmosphere. Although the F_eK_e sink of energy should be less effective in EXP3 compared to EXP2, Fig. 3 shows that the offshore F_eK_{eg} in EXP3 is only slightly larger than the one in EXP2. In EXP3, more EKE is generated in the coastal region that then propagates offshore. As a result there is a larger offshore energetic reservoir, and therefore a larger F_eK_{eg} sink.

A co-spectrum analysis of the total wind work FK and its geostrophic part (FK_g) is performed point-wise for the coastal (30°- 45°N $\times$ d $\leq$ 80 km) and offshore regions ($d > 80\,km$ $\times$ 30°N - and 45°N) (Fig. 7).

F_eK_e and F_eK_eg both show large positive energy input at the low end of the frequency range that are mostly represent the annual cycle of winds acting on the mean California current and surface Ekman velocity. The focus of this study is fairly tiny perturbations from this dominant process that induce a damping of the EKE. Consistent with the previous results, in the coastal region the current feedback to the surface stress reduces the amount of energy input into the ocean between the frequencies 30-$days^{-1}$ and 300-$days^{-1}$ (not shown).

More interestingly, as illustrated in Fig. 7 using EXP1 and EXP3, offshore between 30-$days^{-1}$ and 300-$days^{-1}$, there is a clear FK reduction due to a sink of FK_g, which leads to a transfer of energy from the ocean to the atmosphere. The sink of energy from the geostrophic currents to the atmosphere within the eddy scale band confirms that the current feedback acts as an "eddy killer". As a result, the eddies decay as they propagate offshore and, therefore, are eventually very weak (or absent) very far offshore, explaining the offshore decay of EKE in Fig. 1. Thus, there is a route of energy from the atmosphere to the ocean in the nearshore region, offshore eddy propagation, and then from the offshore eddies to the atmosphere. Finally, in our analysis, the seasonal variability is not removed. At seasonal timescale, the wind has roughly the same direction than the surface currents, so that there is a seasonal positive geostrophic F_eK_e. The same analysis done without the seasonal variability, lead qualitatively to the same results, but with a slightly larger negative F_eK_eg offshore (by 5%). The large values of positive F_eK_e in the nearshore region are also partly driven by the seasonal variability that represents about 30% of the coastal positive F_eK_e (about 30%)..

4. Surface Stress and Wind Response

As reported by Chelton et al. (2007), the link between SST and wind stress in the California upwelling system exhibits a linear relationship between the wind stress curl and the crosswind SST gradient. EXP1 has a wind stress curl - crosswind SST gradient slope of $s_t = 0.019\, m^2\, C^{-1}$ for the summer season, that is similar to the one reported by Chelton et al. (2007). Similar values are found for the other experiments. Here, the focus is on an analogous linear relationship between the surface stress and the oceanic currents, and on the

influence of surface currents on the surface wind speed as apparently not previously been documented.

a. Current-Induced Surface Stress

Similar to Chelton et al. (2007), the statistical relationship between surface stress curl and oceanic current vorticity is evaluated by bin averaging the 1-month running means of the stress curl as a function of the 1-month running means of the oceanic current vorticity over the full simulated period for the three experiments. Bin sizes of $1\,ms^{-1}$ per $100\,km$ and $1\,Nm^{-2}$ per $10^5\,km$ are used for surface current vorticity and the stress curl, respectively. The large scale signal is removed using a high-pass Gaussian spatial filter with a $150\,km$ cut-off. The analysis domain is 30 °N - 45 °N and ($150\,km < d < 500\,km$), *i.e.,* offshore of the wind drop-off region , where the current feedback effects are partly masked by the orographic, coastline, and SST effects on the wind (Perlin et al. 2011; Renault et al. 2015b).

Figure 8 shows the resulting scatterplots. A coupling correlation coefficient s_{st} [$N\ s\ m^{-3}$] is defined as the slope of the linear regression in this scatterplot. Because EXP1 does not consider the surface currents into its surface stress estimate, its wind stress curl does not show any significant dependence on the oceanic vorticity. EXP2 and EXP3 show a clear negative linear relationship between the surface currents vorticity and the surface stress curl, with $s_{st} < 0$. The negative sign is consistent with the $F_e K_{eg}$ sink and Fig. 5, *i.e.,* the current feedback induces an opposite sign surface stress curl. From EXP2 to EXP3 the magnitude of s_{st} decreases significantly. The difference is due to the atmospheric response of an intensification of the surface wind that attenuates the current feedback effect on the surface

stress. Simulations that neglect the wind adjustment to the current feedback (*e.g.,* EXP2 and the North Atlantic simulations of Eden and Dietze (2009)) overestimate the reduction of the surface stress by the oceanic surface currents, missing the partial re-energization of both the atmosphere and ocean through full coupling.

b. Wind Response

The oceanic surface currents partially drive the atmosphere. When coupling the atmosphere to the oceanic currents, the reduction in air-sea velocity difference reduces the stress acting on the wind and allows it to accelerate. Figure 9 depicts the mean cross-shore profiles of surface wind Turbulent Kinetic Energy (TKE) 30°N and 45°N. TKE is always larger in EXP3 than in EXP1, reflecting the changes in surface stress. Interestingly, the nearshore region ($d \leq 80\,km$) has a higher TKE difference than the offshore region. This is likely partly explained by the presence of the steady oceanic geostrophic jet that flows in the same direction as the wind, reducing the surface stress near the coast.

Binned scatterplots of 1-month running means of wind curl and surface current vorticity over the domain 30 °N - 45 °N and ($150\,km < d < 500\,km$) are calculated for EXP1 and EXP3. EXP1, as expected, does not have any significant relationship between wind curl and surface current vorticity (not shown). EXP3 has a clear linear relationship between them (Fig. 10a). An non-dimensional coupling coefficient s_w is defined from the slope of the linear regression estimated from the scatterplot. The positive s_w indicates a positive forcing of the currents on the wind, a positive (negative) current vorticity inducing a positive (negative) wind curl. The wind changes are explained by the surface stress changes, a weaker surface

stress allowing the wind to accelerate. s_w counteracts the effect expressed in s_{st} and hence acts to reduce s_{st} from EXP2 to EXP3. The positive s_w is also consistent with Fig. 5, the currents inducing a positive wind curl in the center of an anticyclonic eddy, that counteracts the current-induced negative surface stress curl. Fig.. 10b depicts the vertical structure of the coupling coefficient s_w. The current feedback mainly shapes the surface wind, however, its effect can be felt up to 300m. Finally, a spectral analysis reveals the current feedback mainly affects the wind at eddy-scale (but can be slightly felt over several hundreds of km.), and over timescale between 30-$days^{-1}$ and 300-$days^{-1}$ (not shown). To our knowledge, this is an entirely new phenomenon that has not previously been pointed out. Finally, although the wind changes have an important effect on the oceanic response, from the atmospheric point of view, the changes are rather small. The Planetary Boundary Layer Height is not changed, nor the mean overlying circulation, the clouds or the precipitations. For more dynamical regions, we expect a larger large scale effect.

5. Induced Ekman Pumping and Eddy Attenuation Time

The current feedback to the atmosphere, by shaping the surface stress, induces an additional Ekman pumping in the ocean which provides a mechanism for weakening an eddy (*i.e.,* the eddy damping by the current feedback). The Ekman pumping is

$$w_{ek} = \boldsymbol{k} \cdot \nabla \times \frac{\boldsymbol{\tau}}{\rho_0 f}\,, \tag{12}$$

where f is the Coriolis frequency. Using the current coupling coefficient s_{st} from EXP3, (12) becomes

$$w_{ek} = \frac{s_{st}\,\Omega_{surf}}{\rho_0\, f}\,. \tag{13}$$

where the surface current vorticity is $\Omega_{surf} = \boldsymbol{k}$. Using (12) and a typical $\Omega_{surf} = 1\times10^{-5}s^{-1}$ on a scale of 100 km, $w_{ek} = 10$ cm day^{-1}, which is similar to the estimate in Gaube et al. (2015).

An attenuation time scale of eddies is then estimated as a result of the current-induced surface stress curl and, to check the results from an energetic point of view, of sink of F_eK_e. In a similar way as described by Gaube et al. (2015), the decay time scale of an eddy associated with the stress curl can be estimated from a simplified vertically-integrated barotropic vorticity balance:

$$\frac{\partial\Omega_{bt}}{\partial t} = \boldsymbol{k}\cdot\nabla_c\times\frac{\boldsymbol{\tau}}{\rho_0}\,. \tag{14}$$

where the eddy barotropic vorticity is defined as the vorticity of the integrated velocities,

$$\Omega_{bt} = \frac{\partial\overline{v}^z}{\partial x} - \frac{\partial\overline{u}^z}{\partial y}\,. \tag{15}$$

$\nabla_c\times\boldsymbol{\tau}$ is the surface stress curl induced by the current feedback, and $\overline{u}^z$ and $\overline{v}^z$ are the zonal and meridional mean depth-averaged current component.

Figure 11 shows a snapshot of the surface current vorticity and a 2000 m vertically integrated current vorticity from EXP3. The integration is not to the bottom is to be able to neglect bottom drag effect on the eddies. At the surface there are small-scale features as filaments that are not present in the depth integral; however, the main eddies can be seen from both the surface vorticity and the depth-integrated vorticity, the depth-integrated vorticity being about 500 larger than the surface vorticity. Therefore, a characteristic vertical

scale of eddies $D = 500m$ can be estimated as a translation between the surface and depth-integrated vorticity:

$$\Omega_{bt} = D\,\Omega_{surf}\,, \tag{16}$$

Using (16) and the current coupling coefficient s_{st}, (14) becomes identical to Eq. (14) of Gaube et al. (2015):

$$\frac{\partial \Omega}{\partial t} = -\frac{f}{D}\,w_{ek}\,. \tag{17}$$

An eddy attenuation time scale can be estimated from (17) as

$$t_{vrt} = \frac{\rho_0\,D}{s_{st}}\,. \tag{18}$$

As previously noted by Gaube *et al.*(2015), this estimate of eddy attenuation time depends only on D, and, in this study, the current coupling coefficient s_{st} and not on the eddy amplitude or radius. Note that s_{st} depends on the background wind that for the CCS is about $5ms^{-1}$. For an eddy with $D = 500m$ under a uniform background wind of $5ms^{-1}$ and using s_{st} from EXP2 ($s_{st} = 0.019N\ s\ m^{-3}$) or from EXP3 ($s_{st} = 0.012N\ s\ m^{-3}$), the eddy attenuation time is $t_{vrt} = 313$ days or $t_{vrt} = 495$ days, respectively. Not surprisingly, when neglecting the atmospheric adjustment, the eddy attenuation time scale is underestimated. Given (18) the shallower the mesoscale eddy is the shorter the eddy attenuation time.

This eddy attenuation time t_{vrt} can be directly compared to the one estimated from the observations by Gaube et al. (2015). From Eq. (19) in Gaube et al. (2015), the wind background here and a surface drag coefficient of $C_d = 0.012$ (Large and Pond 1981), the eddy attenuation time scale is 541 days, which is close to the t_{vrt} in EXP3, *i.e.,* by taking into account the atmospheric adjustment to the current feedback. An eddy attenuation time scale can also be estimated from an energy perspective, in that case, due to the quadratic

form of the EKE, such a timescale is equal to $t_{vrt}/2$ (roughly $250 days$ for EXP3 and $156 days$ for EXP2).

In EXP3 the current feedback reduces the surface EKE by 44% (Fig. 1). However, it only reduces the total integrated EKE by 27%. This is explained by the eddy attenuation time scale that depends on the depth scale of the eddies and on the depth structure of the eddy response. The shallower the eddies are, the more sensitive they are to the current feedback. An alternative interpretation is that the wind damping at the surface changes the vertical structure of the eddies over their lifetime (with the initial structure being set by the baroclinic instability that generates them generally something close to the first baroclinic mode). The anticyclonic eddy observed by (McGillicuddy et al. 2007) and the cyclonic "thinny" described in a recent paper (McGillicuddy Jr 2015) may be examples of this.

6. Eddy Statistics

The eddy tracking method (Sec. 2f) was applied to EXP1, EXP3, and AVISO. Overall, the simulations show a fair agreement with these observations and previous analyses (Chelton et al. 2011; Kurian et al. 2011). Figure 12 shows the eddy sea-surface height (SSH) amplitude and rotational speed distributions. The simulation EXP1 without current feedback overestimates the eddy SSH and rotational speed compared to the observations. It also underestimates the eddy scale, and overestimates the eddy life (not shown), allowing the eddies to propagate further offshore. This is consistent with the too-large offshore EKE in EXP1 (Fig. 1). Due to a reduction of the eddy amplitude, rotational speed, and eddy life (not shown), EXP3 presents a better agreement with the AVISO results through the eddy

killing mechanism.

Recently, Samelson et al. (2014) showed a composite life-cycle for a long-lived mesoscale eddy: on average, the eddy first grows in SSH amplitude, then has a slow growth followed by a slow symmetric decay, and, at the end, the eddy amplitude decreases rapidly before collapsing (see for example Fig. 2 of Samelson et al. 2014). They show a stochastic model was able to predict accurately the eddy life symmetry and thus suggest that the evolution of mesoscale structures is dominated by effectively stochastic interactions, rather than by the classical wave mean cycle of initial growth followed by nonlinear equilibration and barotropic, radiative, or frictional decay, or by the vortex merger processes of inverse turbulent cascade theory. The lengthy stabilization of the composite eddy and its property of symmetry between its growing and decay phases contradicts the results in Gaube et al. (2015) and our own. The eddy should rapidly intensify as it forms, then eventually has a slow growth, but then it should decay in an asymmetric way due the current feedback eddy damping. Figure 13 shows the evolution of the normalized amplitude $\mathcal{A}$ as a function of the normalized time $\mathcal{T}$ for all tracked eddies with a lifetime greater than 16 weeks (*cf.,* Fig. 2 in Samelson et al. (2014)). As in Samelson et al. (2014), each eddy amplitude time series was normalized by its time mean, and the respective lifetime ($\mathcal{L}$) by using the convention $\mathcal{T}1 = 0$ and $\mathcal{T}\mathcal{L} = 1$. In both EXP3 and AVISO, the eddy first grows in strength, then decreases slowly (by 10%) from $\mathcal{T} = 0.3$ to $\mathcal{T} = 0.7$, and finally, decreases rapidly before collapsing (presumably through some destructive interaction with other currents). This supports the current induced eddy killing as a realistic mechanism. In EXP1 the systematic eddy decay during its middle phase seems to be absent. The decay time scale of an eddy associated with the current feedback is also estimated using Fig 13. During the slow decay present in

EXP3 (and not in EXP1), the eddy amplitude is reduced by 10% in roughly $0.4\mathcal{L}$. Using a long-lived eddy mean life of 206 days, a decay time scale t_{eddy} of 527 days is estimated and is consistent with the previous estimation of t_{vrt} and the Gaube et al. (2015) estimate. The discrepancies with the (Samelson et al. 2014) results will need further investigation.

Figures 12-13 do show some discrepancies between EXP3 and AVISO. While no doubt some of these are due to model bias, there are important sampling differences. In particular, the AVISO data has spatial and temporal resolution issues, and sees only the larger mesoscale eddies (Chelton et al. 2011).

7. Discussion and Conclusions

Using coupled ocean-atmosphere simulations, we assess the role of the current feedback through the surface wind work, the energy transfer from the atmosphere to the ocean, and its consequences for both oceanic and atmospheric mesoscale activity. In good agreement with former studies we show the current feedback strongly attenuates the oceanic EKE. A simplified EKE budget shows the current feedback acts on the eddy wind work $F_e K_e$ through its geostrophic component. In the coastal region, it reduces the energy transfer from the atmosphere to the ocean, while offshore it induces a deflection of the energy from the oceanic geostrophic currents (eddies) to the atmosphere. As a results, there is less coastal generation of EKE and damping or even killing of eddies offshore.

The current feedback can be split into two actions: (1) on the surface stress and (2) on the wind. The action on the stress induces the EKE damping, by reducing the energy transfer from the atmosphere to the ocean and even reversing it through the offshore geostrophic

currents. We determine for the U.S. West Coast the coupling coefficients between the oceanic surface current and the surface stress, and between the oceanic surface current and the wind, which are opposing effects. The current feedback has a negative action on the surface stress, a positive (negative) surface vorticity inducing a negative (positive) stress curl. For the first time, we show the wind response to the current feedback partly counteracts the stress effect and therefore partly re-energizes the ocean. In the nearshore region, due to less transfer of energy from the atmosphere to the ocean, the wind accelerates, increasing back the nearshore surface stress and hence the coastal EKE generation. Offshore, there is a positive feedback: a positive surface vorticity inducing a positive wind curl (leading to a positive coupling coefficient), damping the negative current-induced surface stress curl. A simulation that neglects the atmospheric adjustment to the reduced stress (as EXP2 or Eden and Dietze (2009)), systematically overestimates the attenuation of the EKE. There is a route of energy from the atmosphere into the nearshore ocean, offshore energy propagation in the ocean, and then from the offshore ocean to the atmosphere.

Using the current-wind stress coupling coefficient, an eddy attenuation time scale is estimated from a vorticity balance perspective. As shown previously by Gaube et al. (2015), the derived eddy attenuation time scale scale depends on the characteristic vertical scale of the eddies D and the current coupling coefficient s_{st} (which depends on the background wind). Using mean parameters for the CCS, we estimate an eddy attenuation time scale of $t_{vrt} = 495$ days which is consistent with the estimate in Gaube et al. (2015). A simulation that neglects the atmospheric adjustment to the current feedback underestimates the eddy attenuation time scale ($t_{vrt} = 313$ days in that case). We show a similar time scale can be estimated during the slow decay period of the composite average life cycle of long-lived

eddies

Gaube et al. (2015) provides a satellite-based validation of our results. A more direct validation is made here using eddy statistics applied on the coupled simulation without current feedback (*i.e.,* EXP1) and on a fully coupled simulation (*i.e.,* EXP3). Consistent with a reduction of the EKE, the coastal reduction of the energy transfer from the atmosphere to the ocean and the sink of energy from the offshore ocean to the atmosphere actually reduce the eddies amplitude and rotational speed in a realistic way. Simulations that resolve the EKE and without current feedback (*i.e.,* forced by prescribed wind stress or a bulk formula without current feedback) may systematically overestimate the EKE. We also show that the current feedback to the atmosphere also reduces the eddy lifetime in EXP3 and is consistent with the observed composite life-cycle of rapid early intensification, a prolonged middle stage of slow decay due to eddy killing by the current feedback, and an abrupt collapse at the end.

A regional high-resolution atmospheric model is usually very costly compared to an oceanic model. So an important next question is how best to force an uncoupled oceanic model. A simulation that uses prescribed wind stress cannot damp the offshore eddies since the prescribed wind stress is uncorrelated with the eddies. A bulk-forced oceanic simulation, *i.e.,* where the model is forced by the wind, should estimate the surface stress using the relative wind. A distinction is necessary between observations or a fully coupled model, on the one hand, and an uncoupled atmospheric wind product, on the other. For non-deterministic variability (such as oceanic eddies), the bulk formulae used to estimate the surface stress should in any case take into account a parameterization of the partial re-energization of the ocean by the atmospheric response. The surface stress could be estimated with a velocity

559 that is the wind relative to the current corrected by the current-wind coupling coefficient s_w

$$\boldsymbol{U} = \boldsymbol{U_a} - (1 - s_w)\boldsymbol{U_o}, , \tag{19}$$

560 For the U.S.West Coast, $s_w = 0.23$ can be derived from Fig. 10. However, it remains to
561 be seen how well this modified relative wind parameterization would work for an uncoupled
562 model, and the current-wind coupling coefficient found in this study may not be valid for
563 other regions, pending further investigation. The coupling coefficient depends on several
564 local parameters such as the background wind, the steadiness, ane the EKE. Even for the
565 CCS, the wind coupling coefficient may not be accurate for the nearshore region; there the
566 wind adjustment is stronger, canceling more efficiently the reduction of energy transfer from
567 the atmosphere to the ocean. For deterministic features such an adjustment may not be
568 necessary if the model is forced by observations or some adequate representation of the
569 oceanic currents. For instance, for a U.S. West Coast configuration forced by the QuikSCAT
570 wind stress observations (*e.g.,* Capet et al. 2008a; Renault et al. 2015a), the simulated wind-
571 driven alongshore current perturbations may be correlated to the climatological average
572 currents and hence already contain both the atmospheric adjustment to the current feedback
573 and the reduction of the surface stress perturbations, allowing a good agreement of the EKE
574 close to the coast. However, the eddies generated are not correlated with the reality lying
575 behind the measured stress, so that such simulations can not represent the offshore sink
576 of energy from the ocean to the atmosphere, explaining their offshore EKE overestimation.
577 Finally, for low-resolution simulations (*e.g.,* Global Circulation Models), since the EKE is
578 already underestimated, taking into account the current feedback to the atmosphere would
579 induce a larger EKE underestimation, degrading the realism of the simulation.

The current effect on the wind speed should be assessed from the observations. A scatterometer (as QuikSCAT) is fundamentally a stress measuring instrument. The winds are reported as so-called equivalent neutral stability winds, which is the wind that would exist if the conditions were neutrally stable and the ocean current were zero. Therefore, it is not possible to determine from scatterometry alone what the actual surface wind is. Dedicated studies using scatterometer and other observations (*e.g., in situ* ones) should aim to address this issue.

In this study of the CCS, although the perturbations are clearly modulated by the current feedback, the mean surface stress and current are not significantly changed. However, they may be impacted in other regions with stronger currents and or stronger SST fronts, such as the Gulf Stream area. An expanded Lorenz diagram of the depth-integrated energy budget (Lorenz 1955) for the ocean could include a sink of energy by negative geostrophic wind work induced by the current feedback. Consistent with Wang and Huang (2004), the total F_eK_e is much larger than its geostrophic component F_eK_{eg}. Substantial power goes into the surface Ekman currents, (Wang and Huang 2004), and much of this is dissipated within the upper few tens of meter (*i.e.,* in the Ekman layer) and therefore is not available to drive currents and diapycnal mixing deeper in the water column. Two strong pathways of mechanical energy from the surface to the deeper ocean are clear at present: wind forcing of near-inertial oscillations and wind forcing of surface Ekman currents and geostrophic flow (Alford 2003, Watanabe and Hibiya 2002, Scott and Xu 2009)). In EXP3, F_eK_e integrated over the whole domain is an energy conversion of $16.9 \times 10^6\ m^5\, s^{-3}$, whereas F_eK_{eg} is only $2.1 \times 10^6\ m^5\, s^{-3}$. We show the current feedback to the atmosphere mainly acts through the latter. Figure 14 expands the Lorentz diagram of energy conversion for the depth-integrated EKE,

integrated over the whole U.S. West Coast domain during the 1995-1999 period. It includes the geostrophic wind work F_eK_{eg}, and the baroclinic (P_eK_e) and barotropic conversions (K_mK_e). Several energy conversion arrows are added: the current induced eddy geostrophic wind work, $F_eK_{egc} = F_eK_{eg\_EXP1} - F_eK_{eg\_EXP3}$, the current-induced baroclinic conversion, $P_eK_{ec} = P_eK_{e\_EXP1} - P_eK_{e\_EXP3}$, and the current-induced barotropic conversion $K_mK_{ec} = K_mK_{e\_EXP1} - K_mK_{e\_EXP3}$. F_eK_{egc} represents 29% of the total energy input (defined as the sum of F_eK_{eg}, P_eK_e, and K_mK_e), and 43% of F_eK_{eg}. The baroclinic and barotropic conversions adjust to slightly counteract the wind work reduction, inducing a positive power input of 3% of the total eddy energy input. The EKE input is then reduced by 26%, that roughly corresponds to the depth-integrated EKE reduction (27%).

In summary, ocean-atmosphere models should take into account the current feedback to have a realistic representation of the EKE and its associated processes. This might be even more important for biogeochemical models. In the open ocean, and in particular in low-nutrient environments, mesoscale processes increase the net upward flux of limiting nutrients and enhance biological production (Martin and Richards 2001; McGillicuddy et al. 2007; Gaube et al. 2013). McGillicuddy et al. (2007), using observations, show the effects of surface currents on Ekman pumping in eddies and, in particular how it affects the biology. In the EBUS, the eddies modulate biological productivity by subducting nutrients out of the euphotic zone and advecting biogeochemical material offshore (Gruber et al. 2011; Nagai et al. 2015; Renault et al. 2015a). A simulation without current feedback, by overestimating the eddy amplitude, lifetime, and spatial range, may overestimate their quenching and offshore transport effects on the biogeochemical materials. We intend to investigate this soon.

Acknowledgments.

We appreciate support from the Office of Naval Research (ONR N00014-12-1-0939), the National Science Foundation (OCE-1419450), the NASA grants NNX13AD78G and NNX14AM72G, the California Ocean Protection Council grant, and the Bureau of Ocean Energy Management. This work used the Extreme Science and Engineering Discovery Environment (XSEDE) and Yellowstone (NCAR). The authors want to thank two anonymous reviewers and Peter Gaube for their comments, as well as Sebastien Masson and Roger Samelson for useful discussions

REFERENCES

Alford, M. H., 2003: Improved global maps and 54-year history of wind-work on ocean inertial motions. *Geophysical Research Letters*, **30 (8)**.

Beckmann, A. and D. B. Haidvogel, 1993: Numerical simulation of flow around a tall isolated seamount. part i: Problem formulation and model accuracy. *Journal of Physical Oceanography*, **23 (8)**, 1736–1753.

Capet, X., F. Colas, P. Penven, P. Marchesiello, and J. C. McWilliams, 2008a: Eddies in eastern-boundary subtropical upwelling systems. *Ocean Modeling in an Eddying Regime, Geophys. Monogr. Ser*, M. Hecht and H. Hasumi, Eds., AGU, 131–147, doi:10.1029/177GM10.

Capet, X., P. Marchesiello, and J. McWilliams, 2004: Upwelling response to coastal wind profiles. *Geophysical Research Letters*, **31 (13)**.

Capet, X., J. McWilliams, M. Molemaker, and A. Shchepetkin, 2008b: Mesoscale to submesoscale transition in the California Current System. part i: Flow structure, eddy flux, and observational tests. *Journal of Physical Oceanography*, **38 (1)**, 29–43.

Carr, M.-E. and E. J. Kearns, 2003: Production regimes in four Eastern Boundary Current Systems. *Deep Sea Research Part II: Topical Studies in Oceanography*, **50 (22)**, 3199–3221.

Carton, J. A. and B. S. Giese, 2008: A reanalysis of ocean climate using simple ocean data assimilation (soda). *Monthly Weather Review*, **136 (8)**, 2999–3017.

Chaigneau, A., M. Le Texier, G. Eldin, C. Grados, and O. Pizarro, 2011: Vertical structure of mesoscale eddies in the eastern south pacific ocean: A composite analysis from altimetry and argo profiling floats. *Journal of Geophysical Research: Oceans*, **116 (C11)**.

Chelton, D. B., M. G. Schlax, M. H. Freilich, and R. F. Milliff, 2004: Satellite measurements reveal persistent small-scale features in ocean winds. *science*, **303 (5660)**, 978–983.

Chelton, D. B., M. G. Schlax, and R. M. Samelson, 2007: Summertime coupling between sea surface temperature and wind stress in the California Current System. *Journal of Physical Oceanography*, **37 (3)**, 495–517.

Chelton, D. B., M. G. Schlax, and R. M. Samelson, 2011: Global observations of nonlinear mesoscale eddies. *Progress in Oceanography*, **91 (2)**, 167–216.

Chou, M.-D. and M. J. Suarez, 1999: A solar radiation parameterization for atmospheric studies. *NASA Tech. Memo*, **104606**, 40.

Colas, F., X. Capet, J. C. McWilliams, and Z. Li, 2013: Mesoscale eddy buoyancy flux and eddy-induced circulation in Eastern Boundary Currents. *Journal of Physical Oceanography*, **43 (6)**, 1073–1095.

Cornillon, P. and K. Park, 2001: Warm core ring velocities inferred from nscat. *Geophysical research letters*, **28 (4)**, 575–578.

Dawe, J. T. and L. Thompson, 2006: Effect of ocean surface currents on wind stress, heat flux, and wind power input to the ocean. *Geophysical research letters*, **33 (9)**.

Debreu, L., P. Marchesiello, P. Penven, and G. Cambon, 2012: Two-way nesting in split-explicit ocean models: algorithms, implementation and validation. *Ocean Modelling*, **49**, 1–21.

Dewar, W. K. and G. R. Flierl, 1987: Some effects of the wind on rings. *Journal of physical oceanography*, **17 (10)**, 1653–1667.

Ducet, N., P.-Y. Le Traon, and G. Reverdin, 2000: Global high-resolution mapping of ocean circulation from topex/poseidon and ers-1 and-2. *Journal of Geophysical Research-Oceans*, **105 (C8)**, 19 477–19 498.

Duhaut, T. H. and D. N. Straub, 2006: Wind stress dependence on ocean surface velocity: Implications for mechanical energy input to ocean circulation. *Journal of physical oceanography*, **36 (2)**, 202–211.

684 Eden, C. and H. Dietze, 2009: Effects of mesoscale eddy/wind interactions on biological
685 new production and eddy kinetic energy. *Journal of Geophysical Research: Oceans (1978–*
686 *2012)*, **114 (C5)**.

687 Edwards, K. A., A. M. Rogerson, C. D. Winant, and D. P. Rogers, 2001: Adjustment of the
688 marine atmospheric boundary layer to a coastal cape. *Journal of the atmospheric sciences*,
689 **58 (12)**, 1511–1528.

690 FAO, 2009: State of the World's Fisheries and Aquaculture 2008. *Food and Agriculture*
691 *Organization of the United Nations*.

692 Gaube, P., D. B. Chelton, R. M. Samelson, M. G. Schlax, and L. W. ONeill, 2015: Satellite
693 observations of mesoscale eddy-induced ekman pumping. *Journal of Physical Oceanogra-*
694 *phy*, **45 (1)**, 104–132.

695 Gaube, P., D. B. Chelton, P. G. Strutton, and M. J. Behrenfeld, 2013: Satellite observations
696 of chlorophyll, phytoplankton biomass, and ekman pumping in nonlinear mesoscale eddies.
697 *Journal of Geophysical Research: Oceans*, **118 (12)**, 6349–6370.

698 Gruber, N., Z. Lachkar, H. Frenzel, P. Marchesiello, M. Münnich, J. C. McWilliams, T. Na-
699 gai, and G.-K. Plattner, 2011: Eddy-induced reduction of biological production in Eastern
700 Boundary Upwelling Systems. *Nature geoscience*, **4 (11)**, 787–792.

701 Hong, S.-Y. and J.-O. J. Lim, 2006: The wrf single-moment 6-class microphysics scheme
702 (wsm6). *J. Korean Meteor. Soc*, **42 (2)**, 129–151.

703 Hong, S.-Y., Y. Noh, and J. Dudhia, 2006: A new vertical diffusion package with an explicit
704 treatment of entrainment processes. *Monthly Weather Review*, **134 (9)**, 2318–2341.

Hughes, C. W. and C. Wilson, 2008: Wind work on the geostrophic ocean circulation: An observational study of the effect of small scales in the wind stress. *Journal of Geophysical Research: Oceans (1978–2012)*, **113 (C2)**.

Jin, X., C. Dong, J. Kurian, J. C. McWilliams, D. B. Chelton, and Z. Li, 2009: Sst-wind interaction in coastal upwelling: Oceanic simulation with empirical coupling. *Journal of Physical Oceanography*, **39 (11)**, 2957–2970.

Jousse, A., L. Renault, and A. Hall, 2015: Climatic importance of aerosol indirect effects in the northeast pacific. *Submitted to Journal of Climate*.

Kurian, J., F. Colas, X. Capet, J. C. McWilliams, and D. B. Chelton, 2011: Eddy properties in the california current system. *Journal of Geophysical Research: Oceans (1978–2012)*, **116 (C8)**.

Large, W. and S. Pond, 1981: Open ocean momentum flux measurements in moderate to strong winds. *Journal of physical oceanography*, **11 (3)**, 324–336.

Large, W. B., 2006: Surface fluxes for practitioners of global ocean data assimilation. *Ocean Weather Forecasting*, Springer, 229–270.

Large, W. G., J. C. McWilliams, S. C. Doney, et al., 1994: Oceanic vertical mixing: A review and a model with a nonlocal boundary layer parameterization. *Reviews of Geophysics*, **32 (4)**, 363–404.

Lathuilière, C., V. Echevin, M. Lévy, and G. Madec, 2010: On the role of the mesoscale circulation on an idealized coastal upwelling ecosystem. *Journal of Geophysical Research: Oceans (1978–2012)*, **115 (C9)**.

Lemarié, F., 2015: Numerical modification of atmospheric models to include the feedback of oceanic currents on air-sea fluxes in ocean-atmosphere coupled models. Technical Report RT-464, INRIA Grenoble - Rhône-Alpes ; Laboratoire Jean Kuntzmann ; Universite de Grenoble I - Joseph Fourier ; INRIA. URL `https://hal.inria.fr/hal-01184711`.

Lorenz, E. N., 1955: Available potential energy and the maintenance of the general circulation. *Tellus*, **7 (2)**, 157–167.

Marchesiello, P., J. C. McWilliams, and A. Shchepetkin, 2001: Open boundary conditions for long-term integration of regional oceanic models. *Ocean modelling*, **3 (1)**, 1–20.

Marchesiello, P., J. C. McWilliams, and A. Shchepetkin, 2003: Equilibrium structure and dynamics of the California Current System. *Journal of Physical Oceanography*, **33 (4)**, 753–783.

Martin, A. P. and K. J. Richards, 2001: Mechanisms for vertical nutrient transport within a north atlantic mesoscale eddy. *Deep Sea Research Part II: Topical Studies in Oceanography*, **48 (4)**, 757–773.

Mason, E., J. Molemaker, A. F. Shchepetkin, F. Colas, J. C. McWilliams, and P. Sangrà, 2010: Procedures for offline grid nesting in regional ocean models. *Ocean Modelling*, **35 (1)**, 1–15.

McGillicuddy, D. J., et al., 2007: Eddy/wind interactions stimulate extraordinary mid-ocean plankton blooms. *Science*, **316 (5827)**, 1021–1026.

McGillicuddy Jr, D. J., 2015: Formation of intrathermocline lenses by eddy–wind interaction. *Journal of Physical Oceanography*, **45 (2)**, 606–612.

747 Minobe, S., A. Kuwano-Yoshida, N. Komori, S.-P. Xie, and R. J. Small, 2008: Influence of
748 the gulf stream on the troposphere. *Nature*, **452 (7184)**, 206–209.

749 Nagai, T., N. Gruber, H. Frenzel, Z. Lachkar, J. C. McWilliams, and G.-K. Plattner, 2015:
750 Dominant role of eddies and filaments in the offshore transport of carbon and nutrients in
751 the california current system. *Journal of Geophysical Research: Oceans*.

752 Nakanishi, M. and H. Niino, 2006: An improved mellor–yamada level-3 model: Its numer-
753 ical stability and application to a regional prediction of advection fog. *Boundary-Layer*
754 *Meteorology*, **119 (2)**, 397–407.

755 Park, H., D. Lee, W.-P. Jeon, S. Hahn, J. Kim, J. Kim, J. Choi, and H. Choi, 2006: Drag
756 reduction in flow over a two-dimensional bluff body with a blunt trailing edge using a new
757 passive device. *Journal of Fluid Mechanics*, **563**, 389–414.

758 Park, S. and C. S. Bretherton, 2009: The University of Washington shallow convection and
759 moist turbulence schemes and their impact on climate simulations with the community
760 atmosphere model. *Journal of Climate*, **22 (12)**, 3449–3469.

761 Perlin, N., E. D. Skyllingstad, and R. M. Samelson, 2011: Coastal atmospheric circulation
762 around an idealized cape during wind-driven upwelling studied from a coupled ocean-
763 atmosphere model. *Monthly Weather Review*, **139 (3)**, 809–829.

764 Perlin, N., E. D. Skyllingstad, R. M. Samelson, and P. L. Barbour, 2007: Numerical sim-
765 ulation of air-sea coupling during coastal upwelling. *Journal of Physical Oceanography*,
766 **37 (8)**, 2081–2093.

Renault, L., C. Deutsch, J. McWilliams, H. Frenzel, J. Liang, and F. Colas, 2015a: Coastal wind pattern modulates biological productivity in california upwelling. *Submitted to Nature Geoscience*.

Renault, L., B. Dewitte, M. Falvey, R. Garreaud, V. Echevin, and F. Bonjean, 2009: Impact of atmospheric coastal jet off central Chile on sea surface temperature from satellite observations (2000–2007). *Journal of Geophysical Research: Oceans (1978–2012)*, **114 (C8)**.

Renault, L., A. Hall, and J. C. McWilliams, 2015b: Orographic shaping of u.s. west coast wind profiles during the upwelling season. *Climate Dynamics*, 1–17.

Renault, L., et al., 2012: Upwelling response to atmospheric coastal jets off central Chile: A modeling study of the October 2000 event. *Journal of Geophysical Research: Oceans (1978–2012)*, **117 (C2)**.

Saha, S., et al., 2010: The NCEP climate forecast system reanalysis. *Bulletin of the American Meteorological Society*, **91 (8)**, 1015–1057.

Samelson, R., M. Schlax, and D. Chelton, 2014: Randomness, symmetry, and scaling of mesoscale eddy life cycles. *Journal of Physical Oceanography*, **44 (3)**, 1012–1029.

Sandwell, D. T. and W. H. Smith, 1997: Marine gravity anomaly from Geosat and ERS 1 satellite altimetry. *Journal of Geophysical Research: Solid Earth (1978–2012)*, **102 (B5)**, 10 039–10 054.

Scott, R. B. and Y. Xu, 2009: An update on the wind power input to the surface geostrophic flow of the world ocean. *Deep Sea Research Part I: Oceanographic Research Papers*, **56 (3)**, 295–304.

Seo, H., A. J. Miller, and J. R. Norris, 2015: Eddy-wind interaction in the california current system: dynamics and impacts. *Journal of Physical Oceanography*, **(2015)**.

Shchepetkin, A. F. and J. C. McWilliams, 2005: The regional oceanic modeling system (roms): a split-explicit, free-surface, topography-following-coordinate oceanic model. *Ocean Modelling*, **9 (4)**, 347–404.

Shchepetkin, A. F. and J. C. McWilliams, 2009: Correction and commentary for ocean forecasting in terrain-following coordinates: Formulation and skill assessment of the regional ocean modeling system by haidvogel et al., j. comp. phys. 227, pp. 3595–3624. *Journal of Computational Physics*, **228 (24)**, 8985–9000.

Skamarock, W., J. Klemp, J. Dudhia, D. Gill, and D. Barker, 2008: Coauthors, 2008: A description of the Advanced Research wrf version 3. ncar tech. Tech. rep., Note NCAR/TN-4751STR.

Spall, M. A., 2007: Midlatitude wind stress-sea surface temperature coupling in the vicinity of oceanic fronts. *Journal of climate*, **20 (15)**, 3785–3801.

Wang, W. and R. X. Huang, 2004: Wind energy input to the ekman layer*. *Journal of Physical Oceanography*, **34 (5)**, 1267–1275.

Watanabe, M. and T. Hibiya, 2002: Global estimates of the wind-induced energy flux to inertial motions in the surface mixed layer. *Geophysical research letters*, **29 (8)**, 64–1.

Zhang, C., Y. Wang, and K. Hamilton, 2011: Improved representation of boundary layer clouds over the southeast pacific in arw-wrf using a modified tiedtke cumulus parameterization scheme. *Monthly Weather Review*, **139 (11)**, 3489–3513.

List of Tables

1 Sensitivity Experiments 41

TABLE 1. Sensitivity Experiments

Experiments	Current feedback
EXP1	None
EXP2	Only in surface stress, using atmosphere from EXP1
EXP3	In both surface stress and on atmosphere

List of Figures

1 Top panel: Mean surface Eddy Kinetic Energy (EKE, cm^2s^{-2}) from EXP1, EXP2, and EXP3. Bottom panel: Temporal evolution of the EKE averaged over the whole domain. The difference percentages between the uncoupled experiments and the coupled experiment are indicated. There is a reduction of the EKE when using the current to estimate the surface stress. The atmospheric response damps the EKE reduction. From EXP1 to EXP2, the EKE is reduced by 55%, whereas from EXP1 to EXP3, the EKE is reduced by 40%. 49

2 Depth-integrated EKE-budget components (cm^3s^{-3}) from EXP1 (top) and EXP3 (bottom): from left to right: the eddy wind work (F_eK_e), the baroclinic conversion (P_eK_e), and the barotropic conversion (K_mK_e). F_eK_e and P_eK_e are the main energy source terms. The reduction of the EKE in Fig. 1 is explained by the reduction of F_eK_e by the current feedback. 50

3 a) F_eK_e cross-shore profiles (cm^3s^{-3}) averaged between 30°N and 45°N from EXP1 (blue), EXP2 (black), and EXP3 (red), (b) Differences between EXP1 and EXP2 (black), and EXP1 and EXP3 (red). c) same than (a) but for F_eK_{eg}, (d) same than (b) but for the geostrophic eddy wind work F_eK_{eg}. The total differences over the box [30°N and 45°N x d=500 km] between EXP1 and the other experiments are indicated in the legend inlet. Two regions can be distinguished: the coastal region (cross-shore distance $d < 80\,km$), and the offshore region ($d > 80\,km$). In the coastal region, there is a reduction of F_eK_e mainly through its geostrophic component, in the offshore region, there is an actual sink of F_eK_e again through its geostrophic component (F_eK_{eg}). The wind response to the current damps the F_eK_e reduction. 51

4 Geostrophic eddy wind work (F_eK_{eg}) from EXP1 and EXP3. The reduction of F_eK_e is mainly explained by a coastal reduction of F_eK_{eg}, and an offshore sink of energy through F_eK_{eg}. 52

838 5 Schematic representation of the current feedback effects over an anticyclonic
839 eddy, considering a uniform southward wind. The green, black, and blue ar-
840 rows represent the wind, surface stress, and surface current, respectively. The
841 red (blue) shade indicates a positive (negative) F_eK_e. The black (green) +/-
842 signs indicate the current-induced stress (wind) curl. a) A simulation with-
843 out current feedback (*e.g.,* EXP1), b) A simulation that takes into account
844 the current feedback into the estimation of the surface stress but neglects the
845 atmospheric response (*e.g.,* EXP2), and c) A fully coupled simulation, *i.e.,*
846 , that has the current feedback into the surface stress estimate and the at-
847 mospheric response (*e.g.,* EXP3). In EXP1 (*i.e.,* simulations without current
848 feedback), the net F_eK_e is equal to zero. In EXP2 (*i.e.,* simulations with
849 current feedback to the surface stress), over an eddy, the amount of positive
850 wind work (F_eK_e) is reduced and the amount of negative F_eK_e becomes more
851 negative. As a result, the net F_eK_e becomes negative, deflecting energy out
852 of the eddy to the atmosphere. In a fully coupled model (EXP3), the atmo-
853 spheric response damps the sink of F_eK_e by increasing the positive F_eK_e and
854 decreasing the negative F_eK_e, the net F_eK_e remaining negative. The current
855 feedback induces a positive (negative) stress curl (wind curl) in the eddy's
856 center. 53

857 6 Schematic representation of the current feedback considering a uniform south-
858 ward wind blowing along the coast. a) A simulation without current feedback
859 (*e.g.,* EXP1), b) A simulation that takes into account the current feedback
860 into the estimation of the surface stress but neglects the atmospheric response
861 (*e.g.,* EXP2), and c) A fully coupled simulation, *i.e.,* that has the current feed-
862 back into the stress estimate and the atmospheric response (*e.g.,* EXP3). The
863 green, black, and blue arrows represent the wind, surface stress, and oceanic
864 surface current, respectively. The red shade represents the induced $F_e K_e$ (pos-
865 itive in all cases). The wind induces an oceanic coastal geostrophic jet that
866 is partially in the same as direction than the wind, inducing a positive $F_e K_e$.
867 From EXP1 to EXP2, the reduction of the stress induces in turn a weakening
868 of $F_e K_e$. From EXP2 to EXP3, the wind accelerates, increasing back toward
869 its initial value the surface stress and hence $F_e K_e$ and the oceanic coastal
870 geostrophic jet. 54

871 7 a) Temporal 1D co-spectrum of the total wind work FK from EXP1 and EXP3
872 between 30°N and 45°N for the offshore region ($d > 80\,km$), b) Difference
873 between EXP1 and EXP3. c) Same than (a) but for the geostrophic wind
874 work, d) same as b) for the geostrophic wind work. The current feedback to
875 the atmosphere act as an eddy killer by reducing $F_e K_e$ through its geostrophic
876 component, deflecting energy from the ocean to the atmosphere. 55

8 Binned scatterplot of the full time series of 1-month running means of surface stress curl and surface current vorticity over the domain 30 °N - 45 °N and $(150\,km < d < 500km)$. The bars indicate plus and minus one the standard deviation about the average drawn by stars. The linear regression is indicated by a black line and the slope s_{st} is indicated in the title $(10^{-2}\,N\,s\,m^{-3})$. From the left to the right: EXP1, EXP2, and EXP3. EXP1 does not have a significant slope since it does not have the current feedback to the atmosphere nor the surface stress. EXP2 and EXP3 presents a clear negative linear relationship between the currents and the stress curl. The currents feedback induce fine scale wind stress structure. Consistently with the previous results, the atmospheric response reduces the current feedback effect on the stress. 56

9 a) Cross-shore profile of the Turbulent Kinetic Energy (TKE) of the surface wind averaged between 30°N and 45°N from EXP1 (cyan) and EXP3 (red). The F_eK_e sink from the ocean to the atmosphere results in a slightly larger TKE in EXP3 compared to EXP1. In the nearshore region, there is a larger wind enhancement that is likely partly explained by the presence of the steady oceanic geostrophic jet that flows in the same direction as the wind. 57

10 a) Same as Fig. 8 but for the wind curl and the surface current vorticity for EXP3. There is a positive linear relationship between the current vorticity and the wind curl, *i.e.,* the current feedback on the atmosphere induces fine scale structures in the wind field that counteract the current-induced stress structure (Fig. 8). This explains the damping of the current feedback effect on the EKE (see text). The linear regression is indicated by a black line and the dimensionless slope s_w is indicated in the title. b) Vertical attenuation of s_w with respect to the surface s_w. 58

11 a) Snapshot of sea surface relative vorticity and b) 2000 m integrated relative vorticity, from EXP3. The colorbar scale is adjusted between (a) and (b) by a factor of $D = 500$ that allows to have a rough match between the two panels. D factor is interpreted as the characteristic vertical scale of the eddies. 59

12 Long-lived (16 weeks) eddy amplitude and rotational speed statistics from EXP1 (blue), EXP3 (red), and AVISO (green). Consistently with the previous results, the current feedback to the atmosphere damps the eddy amplitude and rotational speed, improving the realism of the simulation. 60

13 Evolution of eddy normalized amplitude $\mathcal{A}$ as a function of their dimensionless time $\mathcal{T}$ for all tracked eddies with a lifetime greater than 16 weeks. The blue, red, and green colors represent the results from EXP1, EXP3, and AVISO. In EXP3, consistently with AVISO, the eddy first grows in size, then, due to the current feedback to the atmosphere, decreases slowly, and finally, decreases rapidly before collapsing. In EXP1, the slow decrease is not evident. 61

916 14 An expanded Lorenz diagram of energy conversion for the depth-integrated
917 EKE, integrated over the whole U.S. West Coast domain for the period 1995-
918 1999. The atmosphere is above and mean ocean KE and PE to the left (not
919 represented). The current feedback to the atmosphere mainly removes energy
920 from the ocean to the atmosphere through the geostrophic flow. The mean
921 integrated values for each conversion term are indicated in $m^5\,s^{-3}$. ϵ is the
922 dissipation term, and BF the energy flux o through the boundary. See text
923 for more information. 62

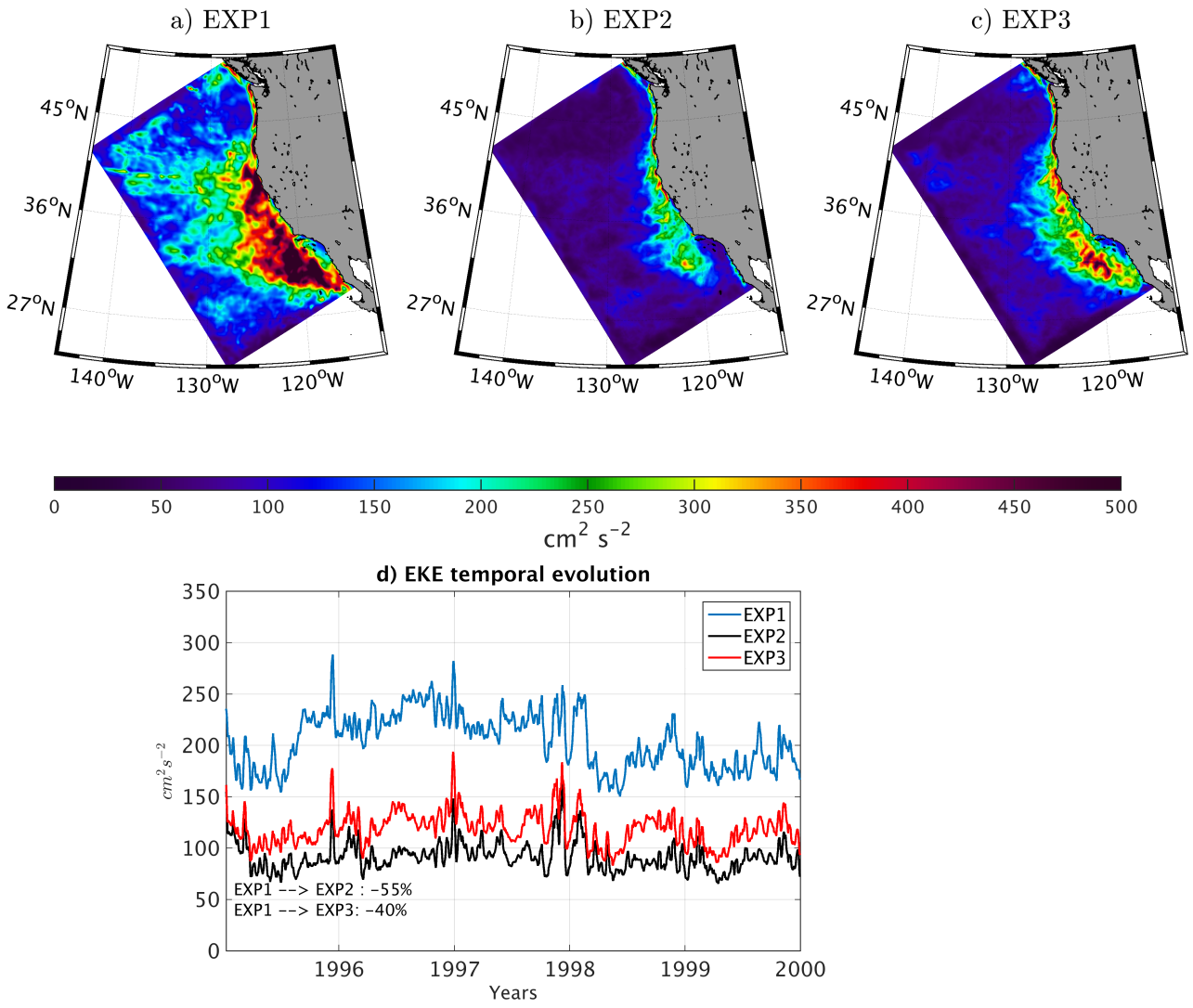

FIG. 1. Top panel: Mean surface Eddy Kinetic Energy (EKE, cm^2s^{-2}) from EXP1, EXP2, and EXP3. Bottom panel: Temporal evolution of the EKE averaged over the whole domain. The difference percentages between the uncoupled experiments and the coupled experiment are indicated. There is a reduction of the EKE when using the current to estimate the surface stress. The atmospheric response damps the EKE reduction. From EXP1 to EXP2, the EKE is reduced by 55%, whereas from EXP1 to EXP3, the EKE is reduced by 40%.

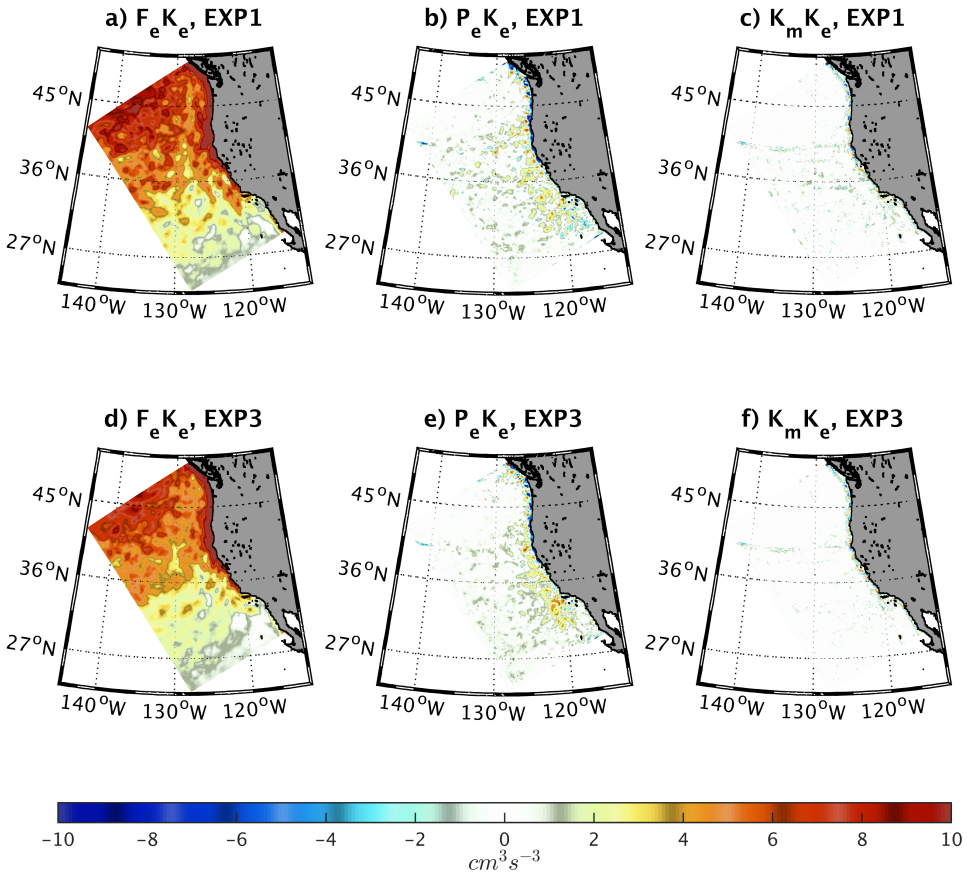

FIG. 2. Depth-integrated EKE-budget components (cm^3s^{-3}) from EXP1 (top) and EXP3 (bottom): from left to right: the eddy wind work (F_eK_e), the baroclinic conversion (P_eK_e), and the barotropic conversion (K_mK_e). F_eK_e and P_eK_e are the main energy source terms. The reduction of the EKE in Fig. 1 is explained by the reduction of F_eK_e by the current feedback.

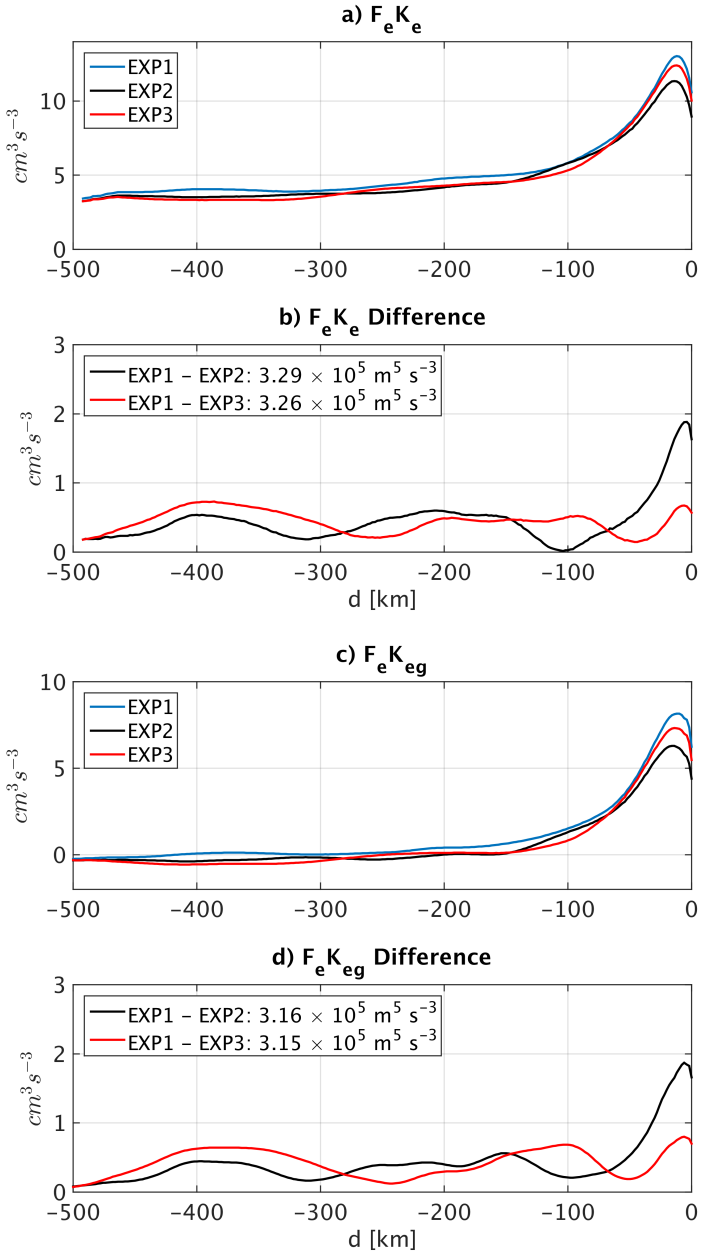

FIG. 3. a) F_eK_e cross-shore profiles (cm^3s^{-3}) averaged between 30°N and 45°N from EXP1 (blue), EXP2 (black), and EXP3 (red), (b) Differences between EXP1 and EXP2 (black), and EXP1 and EXP3 (red). c) same than (a) but for F_eK_{eg}, (d) same than (b) but for the geostrophic eddy wind work F_eK_{eg}. The total differences over the box [30°N and 45°N x d=500 km] between EXP1 and the other experiments are indicated in the legend inlet. Two regions can be distinguished: the coastal region (cross-shore distance $d < 80\,km$), and the offshore region ($d > 80\,km$). In the coastal region, there is a reduction of F_eK_e mainly through its geostrophic component, in the offshore region, there is an actual sink of F_eK_e again through its geostrophic component (F_eK_{eg}). The wind response to the current damps the F_eK_e reduction.

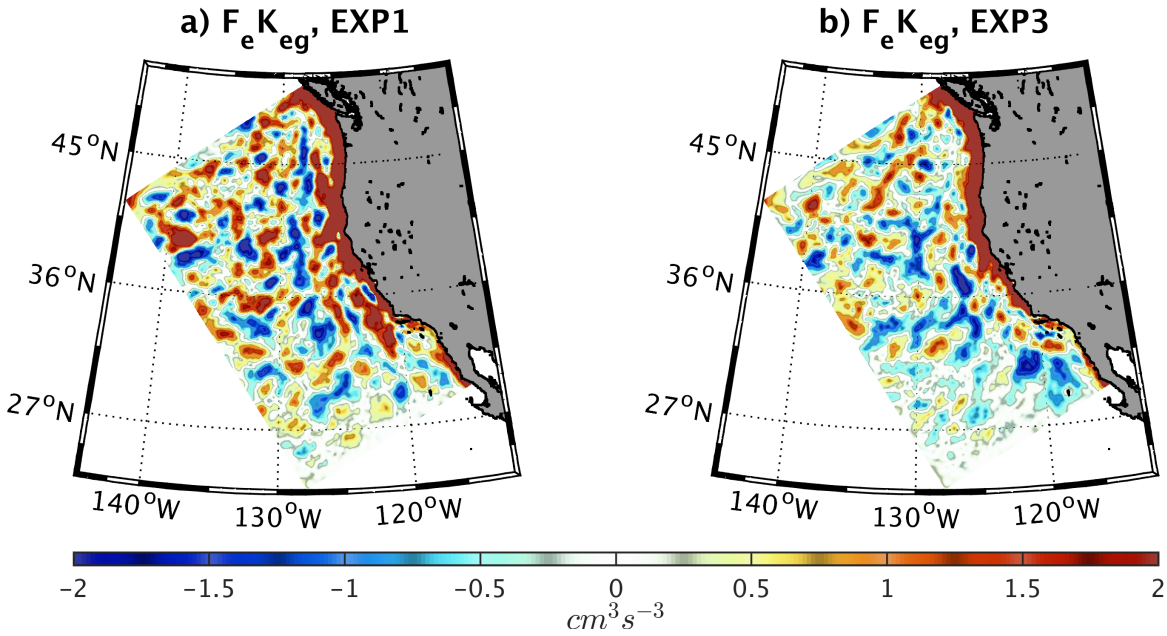

FIG. 4. Geostrophic eddy wind work (F_eK_{eg}) from EXP1 and EXP3. The reduction of F_eK_e is mainly explained by a coastal reduction of F_eK_{eg}, and an offshore sink of energy through F_eK_{eg}.

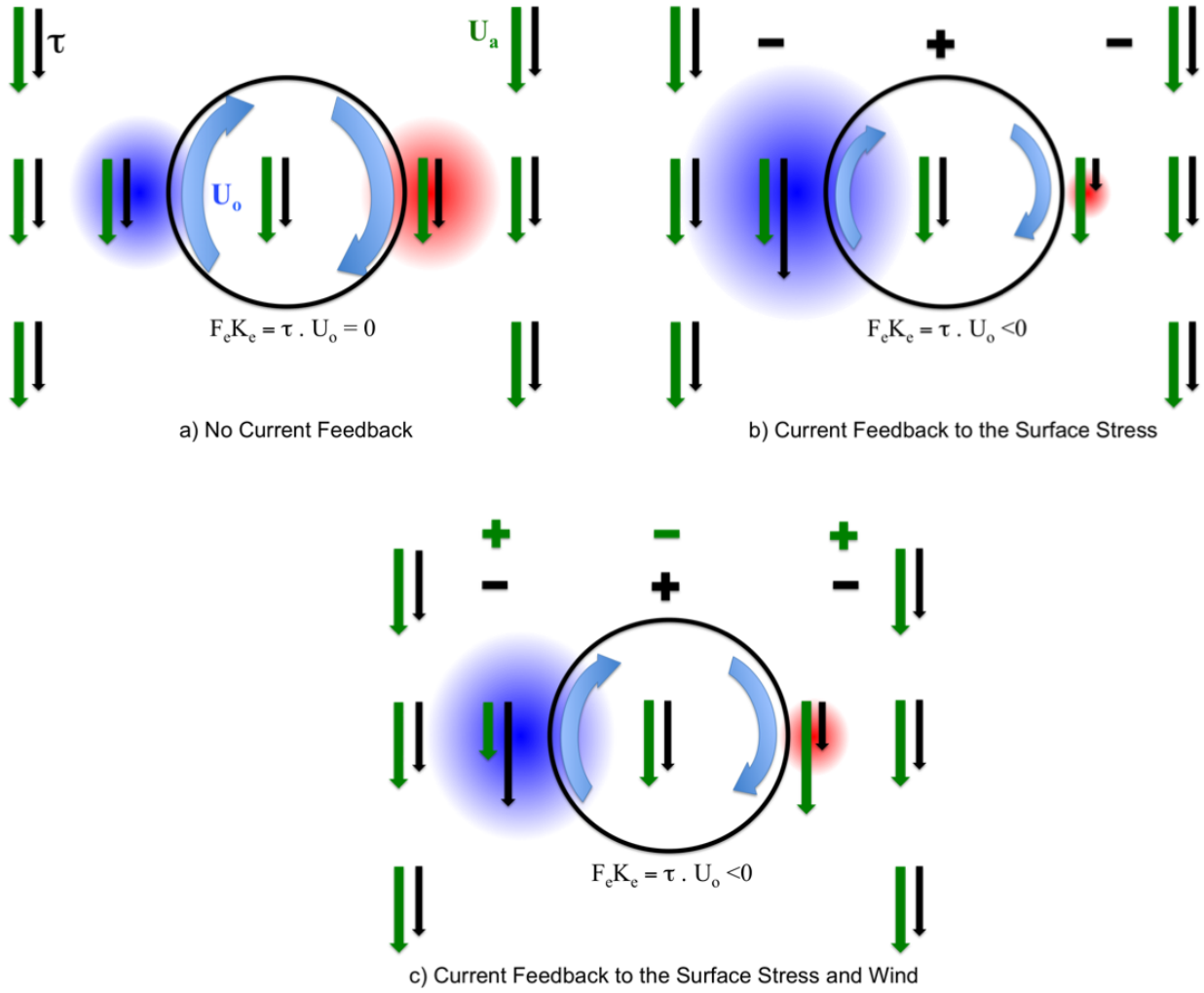

FIG. 5. Schematic representation of the current feedback effects over an anticyclonic eddy, considering a uniform southward wind. The green, black, and blue arrows represent the wind, surface stress, and surface current, respectively. The red (blue) shade indicates a positive (negative) F_eK_e. The black (green) +/- signs indicate the current-induced stress (wind) curl. a) A simulation without current feedback (*e.g.,* EXP1), b) A simulation that takes into account the current feedback into the estimation of the surface stress but neglects the atmospheric response (*e.g.,* EXP2), and c) A fully coupled simulation, *i.e.,* , that has the current feedback into the surface stress estimate and the atmospheric response (*e.g.,* EXP3). In EXP1 (*i.e.,* simulations without current feedback), the net F_eK_e is equal to zero. In EXP2 (*i.e.,* simulations with current feedback to the surface stress), over an eddy, the amount of positive wind work (F_eK_e) is reduced and the amount of negative F_eK_e becomes more negative. As a result, the net F_eK_e becomes negative, deflecting energy out of the eddy to the atmosphere. In a fully coupled model (EXP3), the atmospheric response damps the sink of F_eK_e by increasing the positive F_eK_e and decreasing the negative F_eK_e, the net F_eK_e remaining negative. The current feedback induces a positive (negative) stress curl (wind curl) in the eddy's center.

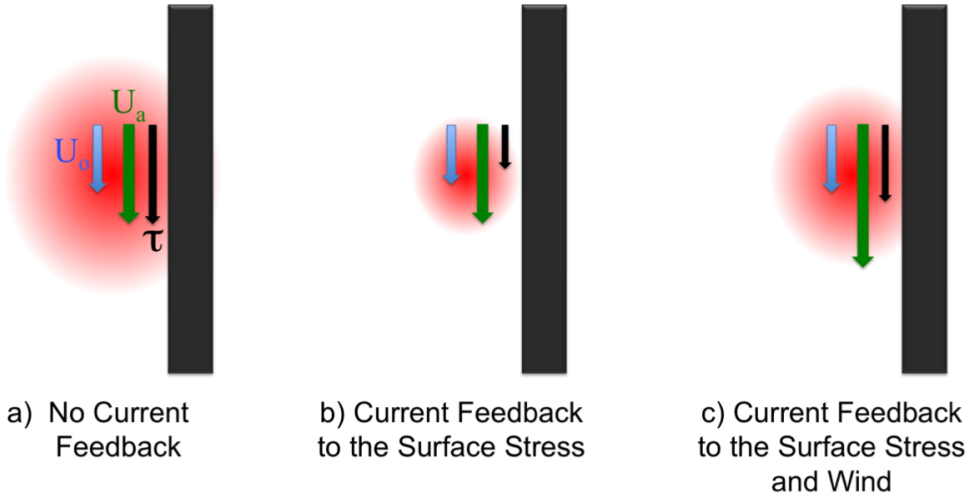

FIG. 6. Schematic representation of the current feedback considering a uniform southward wind blowing along the coast. a) A simulation without current feedback (*e.g.,* EXP1), b) A simulation that takes into account the current feedback into the estimation of the surface stress but neglects the atmospheric response (*e.g.,* EXP2), and c) A fully coupled simulation, *i.e.,* that has the current feedback into the stress estimate and the atmospheric response (*e.g.,* EXP3). The green, black, and blue arrows represent the wind, surface stress, and oceanic surface current, respectively. The red shade represents the induced $F_e K_e$ (positive in all cases). The wind induces an oceanic coastal geostrophic jet that is partially in the same as direction than the wind, inducing a positive $F_e K_e$. From EXP1 to EXP2, the reduction of the stress induces in turn a weakening of $F_e K_e$. From EXP2 to EXP3, the wind accelerates, increasing back toward its initial value the surface stress and hence $F_e K_e$ and the oceanic coastal geostrophic jet.

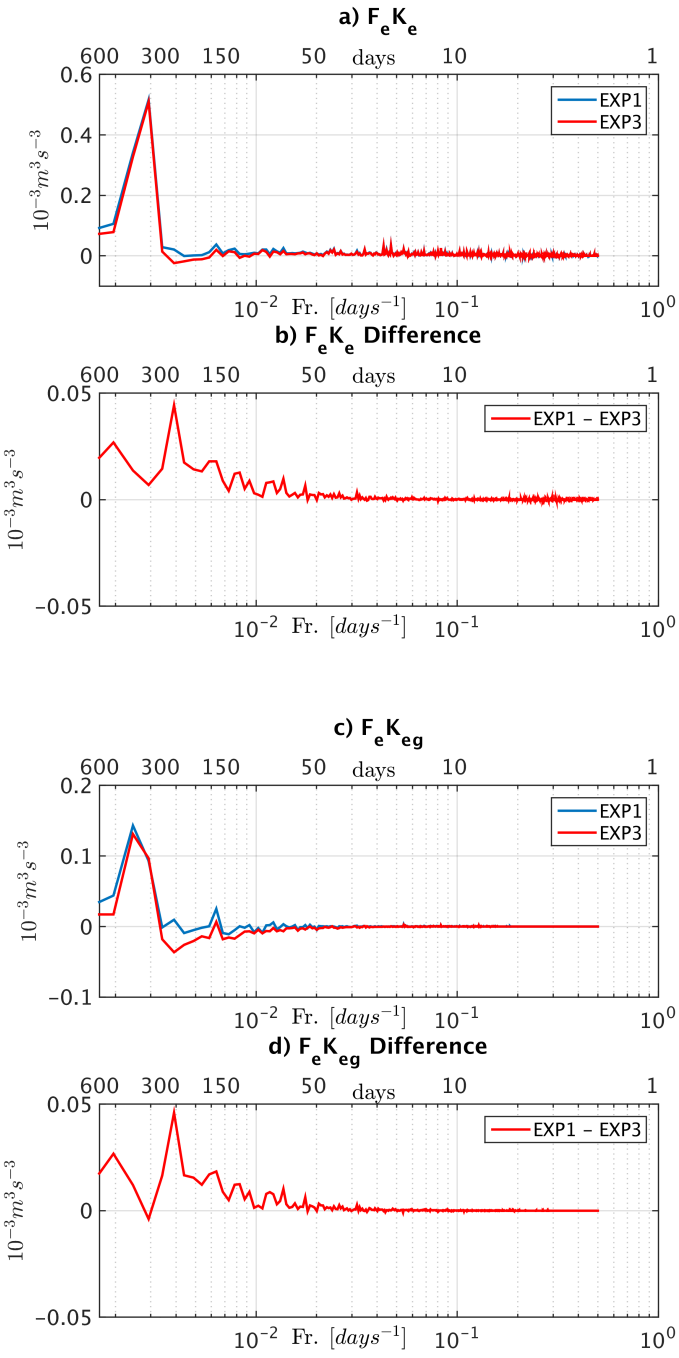

FIG. 7. a) Temporal 1D co-spectrum of the total wind work FK from EXP1 and EXP3 between 30°N and 45°N for the offshore region ($d > 80\,km$), b) Difference between EXP1 and EXP3. c) Same than (a) but for the geostrophic wind work, d) same as b) for the geostrophic wind work. The current feedback to the atmosphere act as an eddy killer by reducing F_eK_e through its geostrophic component, deflecting energy from the ocean to the atmosphere.

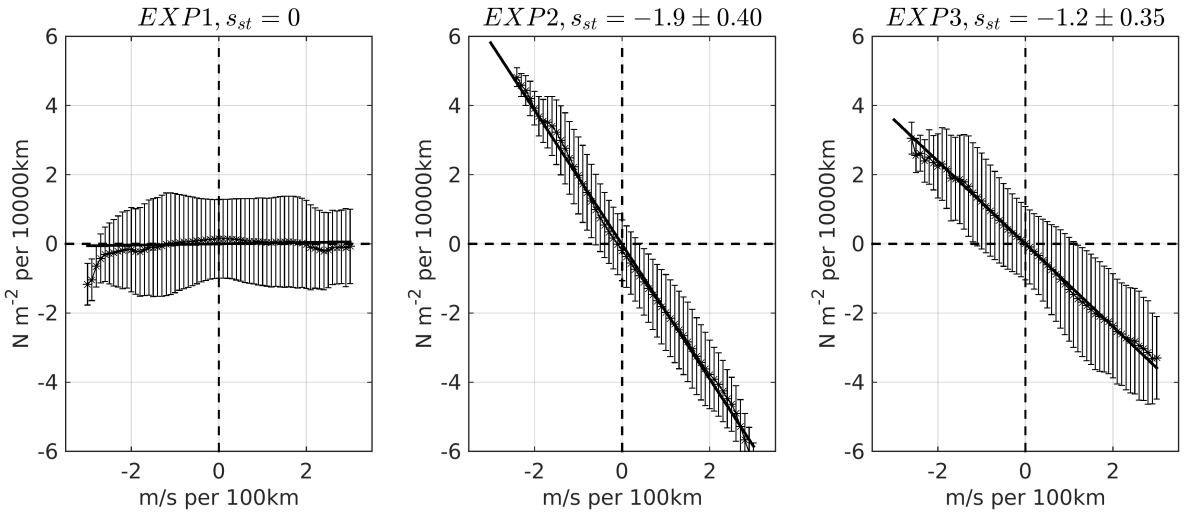

FIG. 8. Binned scatterplot of the full time series of 1-month running means of surface stress curl and surface current vorticity over the domain 30 °N - 45 °N and ($150\,km < d < 500km$). The bars indicate plus and minus one the standard deviation about the average drawn by stars. The linear regression is indicated by a black line and the slope s_{st} is indicated in the title ($10^{-2}\,N\,s\,m^{-3}$). From the left to the right: EXP1, EXP2, and EXP3. EXP1 does not have a significant slope since it does not have the current feedback to the atmosphere nor the surface stress. EXP2 and EXP3 presents a clear negative linear relationship between the currents and the stress curl. The currents feedback induce fine scale wind stress structure. Consistently with the previous results, the atmospheric response reduces the current feedback effect on the stress.

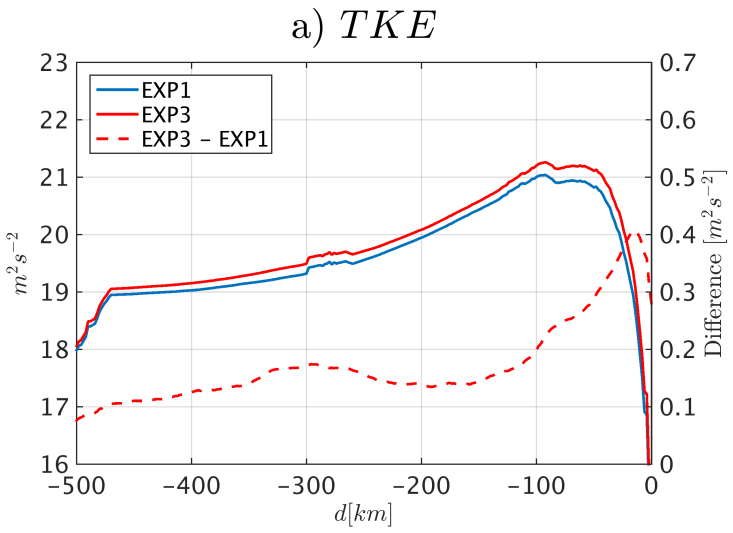

FIG. 9. a) Cross-shore profile of the Turbulent Kinetic Energy (TKE) of the surface wind averaged between 30°N and 45°N from EXP1 (cyan) and EXP3 (red). The F_eK_e sink from the ocean to the atmosphere results in a slightly larger TKE in EXP3 compared to EXP1. In the nearshore region, there is a larger wind enhancement that is likely partly explained by the presence of the steady oceanic geostrophic jet that flows in the same direction as the wind.

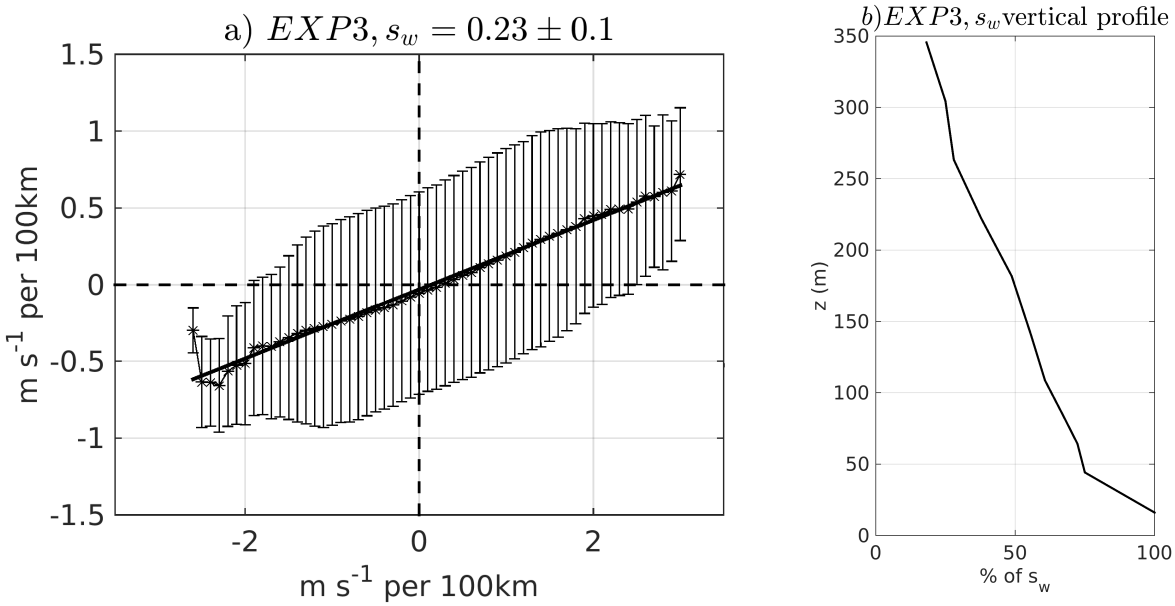

FIG. 10. a) Same as Fig. 8 but for the wind curl and the surface current vorticity for EXP3. There is a positive linear relationship between the current vorticity and the wind curl, *i.e.,* the current feedback on the atmosphere induces fine scale structures in the wind field that counteract the current-induced stress structure (Fig. 8). This explains the damping of the current feedback effect on the EKE (see text). The linear regression is indicated by a black line and the dimensionless slope s_w is indicated in the title. b) Vertical attenuation of s_w with respect to the surface s_w.

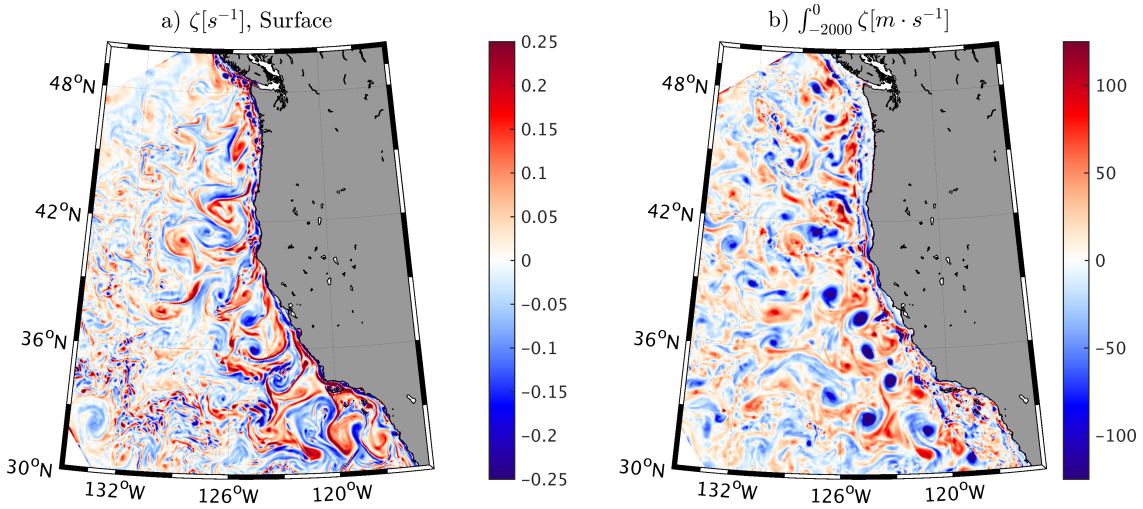

FIG. 11. a) Snapshot of sea surface relative vorticity and b) 2000 m integrated relative vorticity, from EXP3. The colorbar scale is adjusted between (a) and (b) by a factor of $D = 500$ that allows to have a rough match between the two panels. D factor is interpreted as the characteristic vertical scale of the eddies.

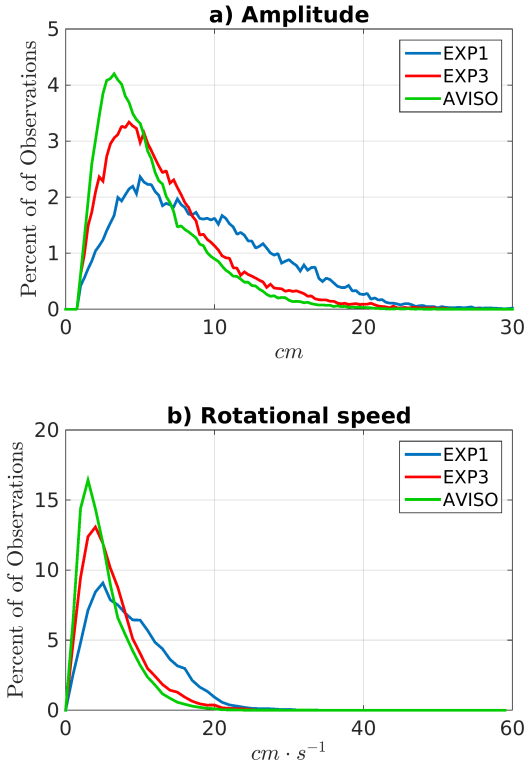

FIG. 12. Long-lived (16 weeks) eddy amplitude and rotational speed statistics from EXP1 (blue), EXP3 (red), and AVISO (green). Consistently with the previous results, the current feedback to the atmosphere damps the eddy amplitude and rotational speed, improving the realism of the simulation.

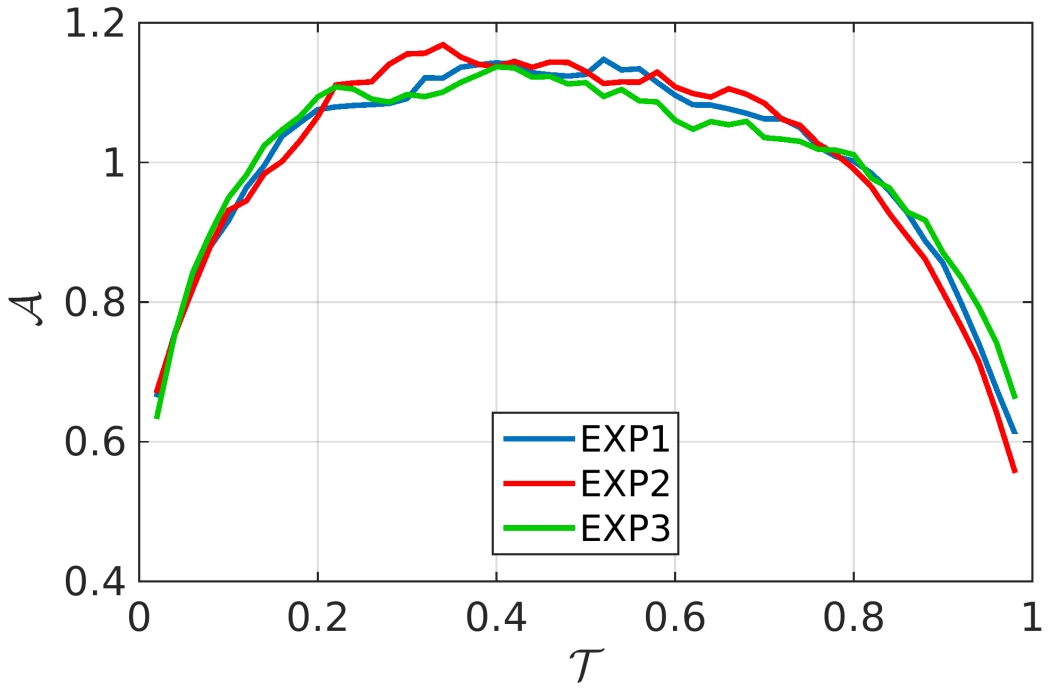

FIG. 13. Evolution of eddy normalized amplitude $\mathcal{A}$ as a function of their dimensionless time $\mathcal{T}$ for all tracked eddies with a lifetime greater than 16 weeks. The blue, red, and green colors represent the results from EXP1, EXP3, and AVISO. In EXP3, consistently with AVISO, the eddy first grows in size, then, due to the current feedback to the atmosphere, decreases slowly, and finally, decreases rapidly before collapsing. In EXP1, the slow decrease is not evident.

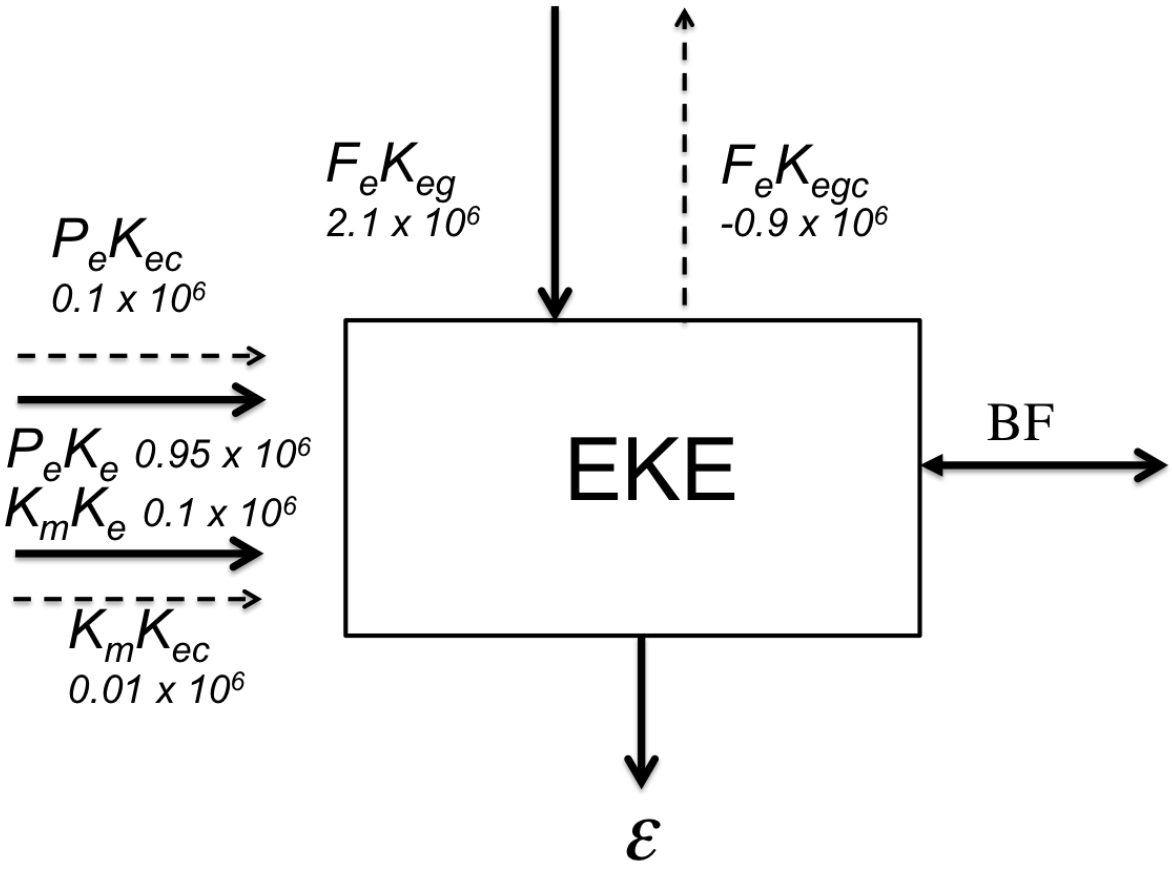

FIG. 14. An expanded Lorenz diagram of energy conversion for the depth-integrated EKE, integrated over the whole U.S. West Coast domain for the period 1995-1999. The atmosphere is above and mean ocean KE and PE to the left (not represented). The current feedback to the atmosphere mainly removes energy from the ocean to the atmosphere through the geostrophic flow. The mean integrated values for each conversion term are indicated in $m^5\,s^{-3}$. ϵ is the dissipation term, and BF the energy flux o through the boundary. See text for more information.